Diastereoselective Alkylation of β-Amino Esters: Structural and Rate Studies Reveal Alkylations of Hexameric Lithium Enolates

Anne J. McNeil,† Gilman E. S. Toombes,‡ Sol M. Gruner,‡ Emil Lobkovsky,† David B. Collum,*,† Sithamalli V. Chandramouli,§ Benoit J. Vanasse,§ and Timothy A. Ayers§

Contribution from the †Department of Chemistry and Chemical Biology, Baker Laboratory, Cornell University, Ithaca, New York 14853-1301, ‡Physics Department, Clark Hall, Cornell University, Ithaca, New York 14853-2501, and §Aventis, Process Development Chemistry, Bridgewater, New Jersey 08807

MNDO Computations

Mathematical Derivations

Structure Chart

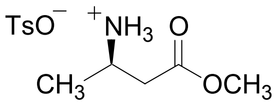

2

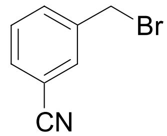

3
($ArCH_2Br$)

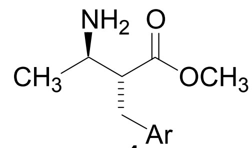

4

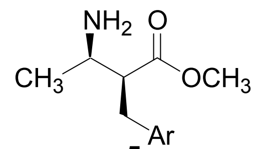

5

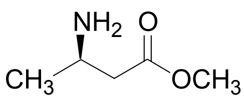

(*R*)-**6**

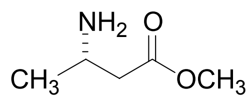

(*S*)-**6**

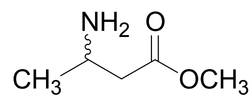

rac-**6**

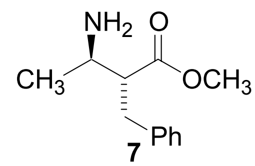

7

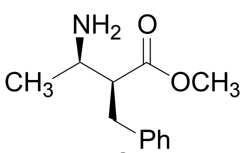

8

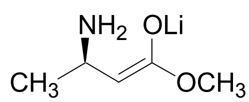

(*R*)-**9**

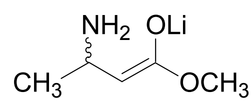

rac-**9**

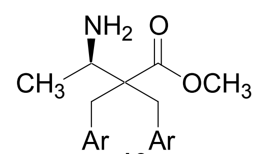

10

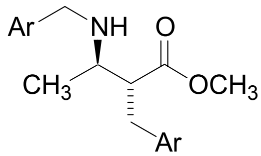

11

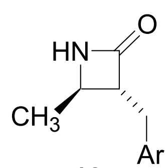

12

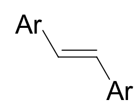

13

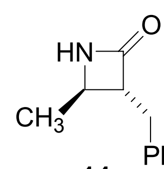

14

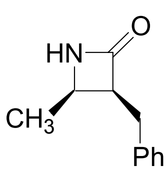

15

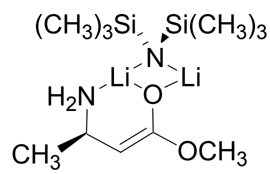

27

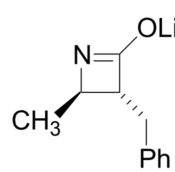

28

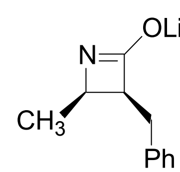

29

Spectroscopic Data for Characterization

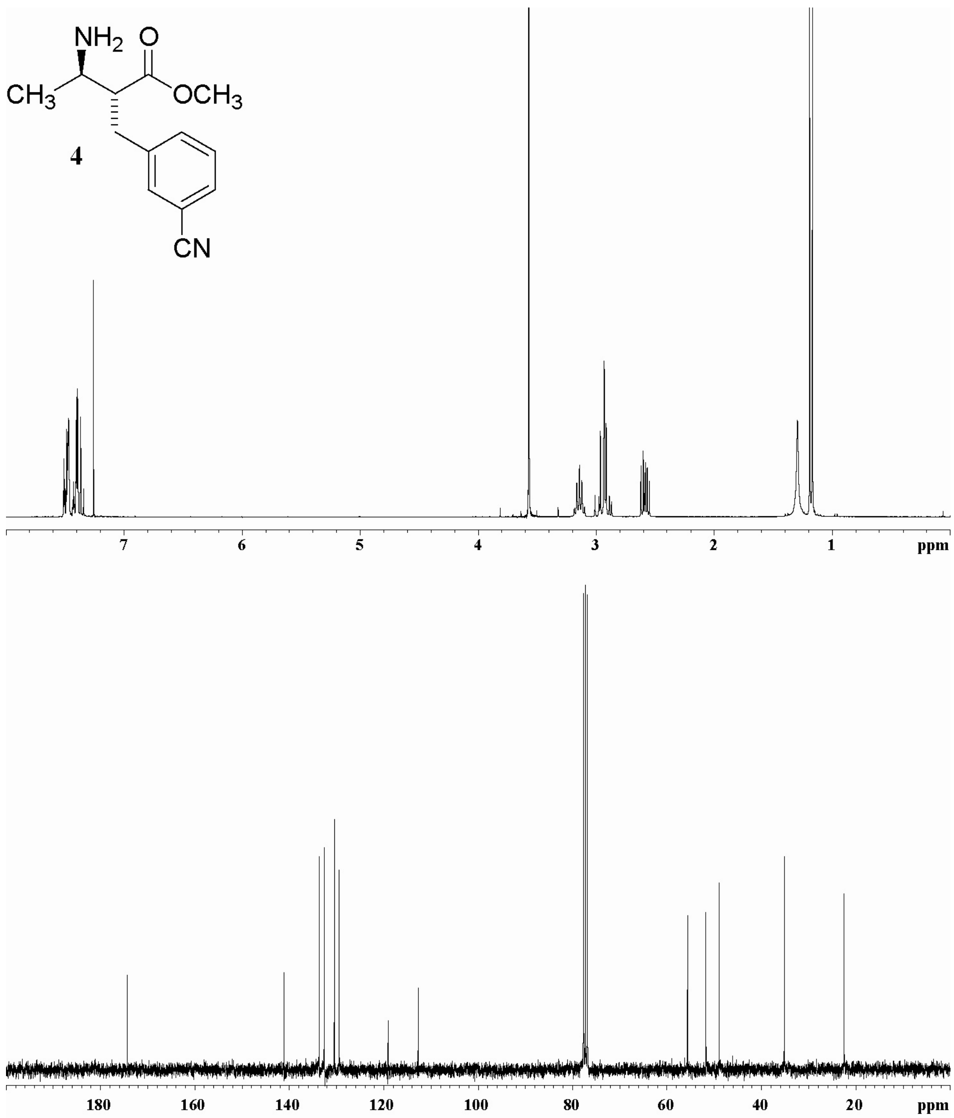

1. ^{1}H NMR (300 MHz, $CDCl_3$): δ 1.17 (d, J = 6.5 Hz, 3H), 1.27 (bs, 2H), 2.54-2.62 (m, 1H), 2.89 (dd, J = 5.7, 13.5 Hz, 1H), 2.97 (dd, J = 10, 13.2 Hz, 1H), 3.14 (pentet, J = 6.3 Hz, 1H), 3.56 (s, 3H), 7.26-7.48 (m, 4H). ^{13}C NMR (75 MHz, $CDCl_3$): δ 22.5, 35.1, 48.9, 51.8, 55.6, 112.7, 119.1, 129.5, 130.5, 132.6, 133.6, 141.1, 174.3.

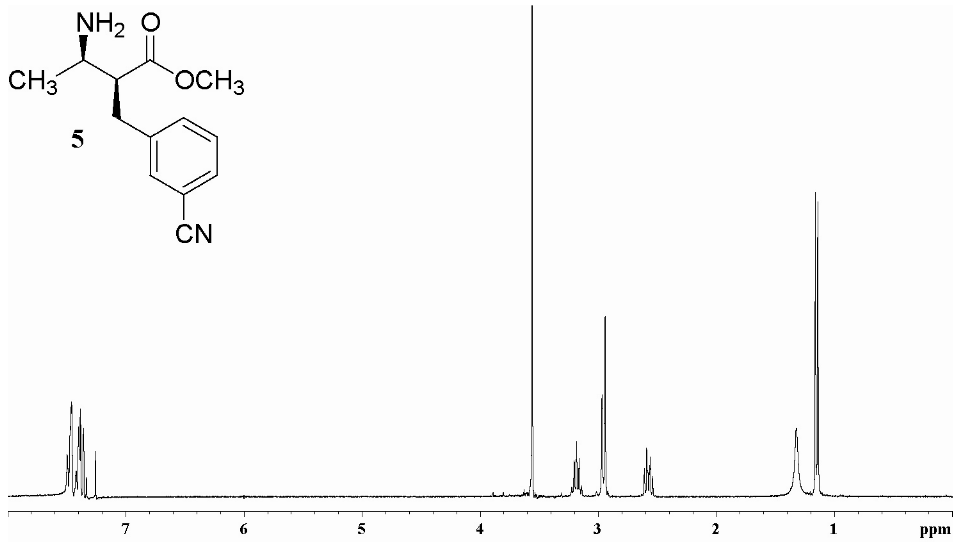

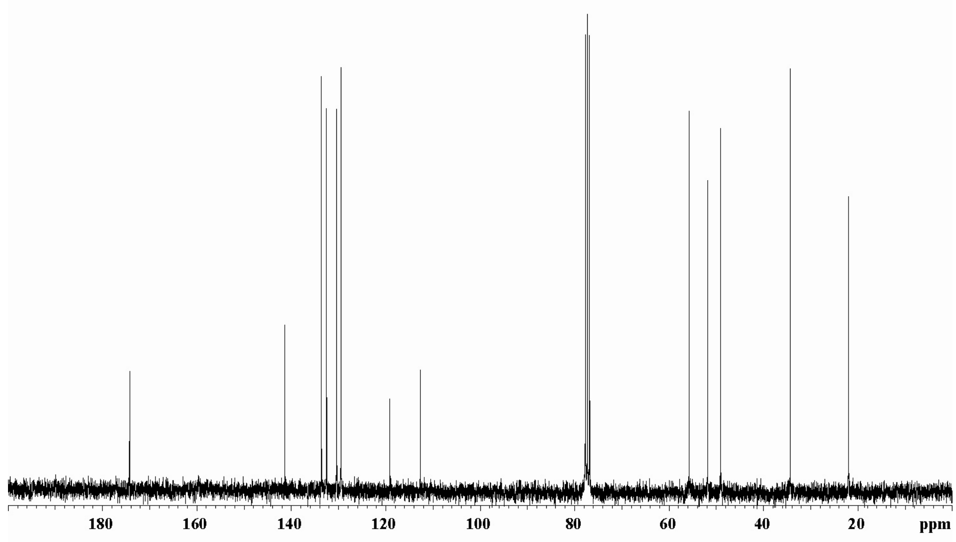

2. ^{1}H NMR (300 MHz, CDCl$_3$): δ 1.15 (d, J = 6.6 Hz, 3H), 1.32 (bs, 2H), 2.54-2.61 (m, 1H), 2.92-3.02 (m, 1H), 3.18 (pentet, J = 6.3 Hz, 1H), 3.56 (s, 3H), 7.26-7.50 (m, 4H). ^{13}C NMR (75 MHz, CDCl$_3$): δ 21.9, 34.3, 49.0, 51.8, 55.7, 112.7, 119.1, 129.5, 130.4, 132.5, 133.6, 141.4, 174.3.

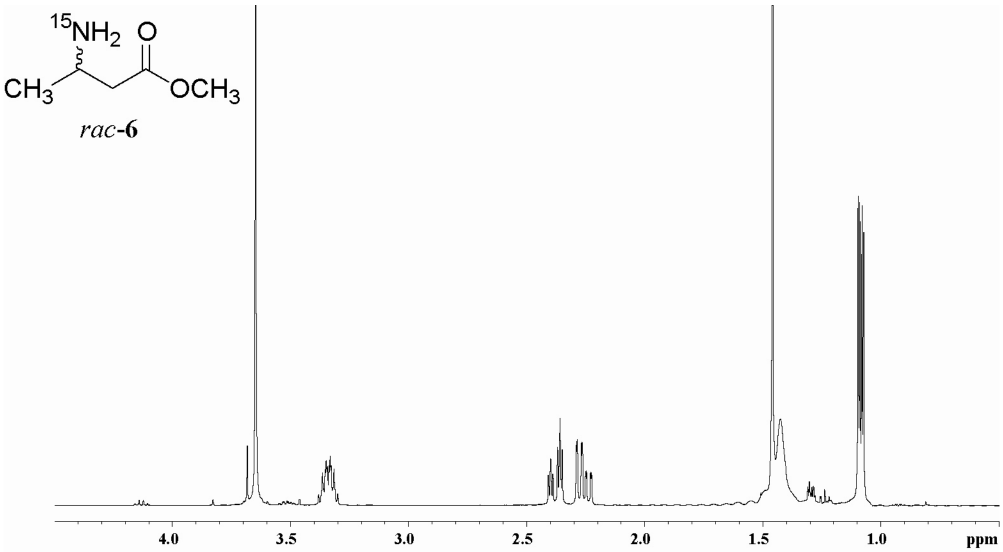

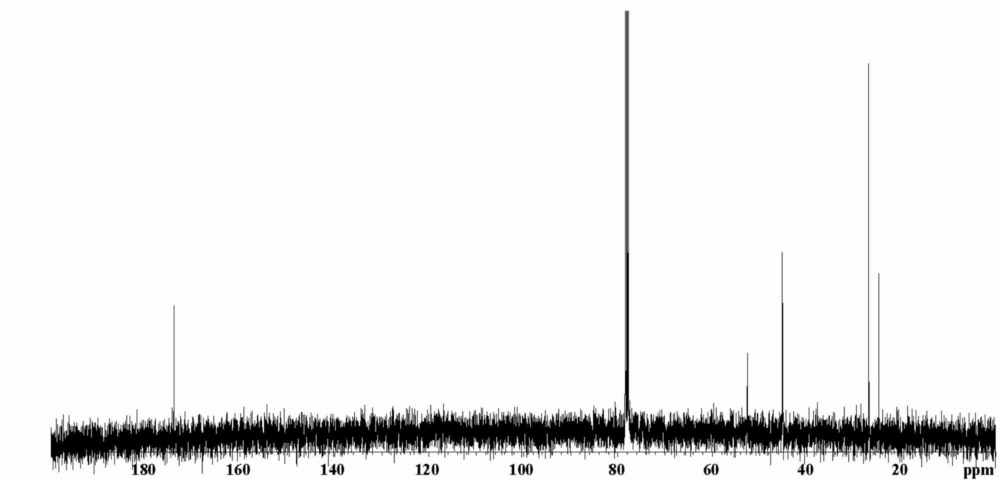

3. ^{1}H NMR (400 MHz, $CDCl_3$): δ 1.08 (dd, J = 2.8, 6.6 Hz, 3H), 1.43 (bs, 2H), 1.46 (C_5H_{10}), 2.28 (dd, J = 8, 16 Hz, 1 H) 2.38 (m, 1H), 3.3-3.4 (m, 1H), 3.65 (s, 3H). ^{13}C NMR (100 MHz, $CDCl_3$): δ 24.7, 26.9 (C_5H_{10}), 45.08, 45.14, 52.6, 173.9. (Note: C_5H_{10} is the solvent cyclopentane.)

^{15}N-labeled β-amino esters were synthesized from [^{15}N]alanine via the Arndt-Eistert protocol. (Podlech, J.; Seebach, D. *Liebigs Ann.* **1995**, 1217-1228.)

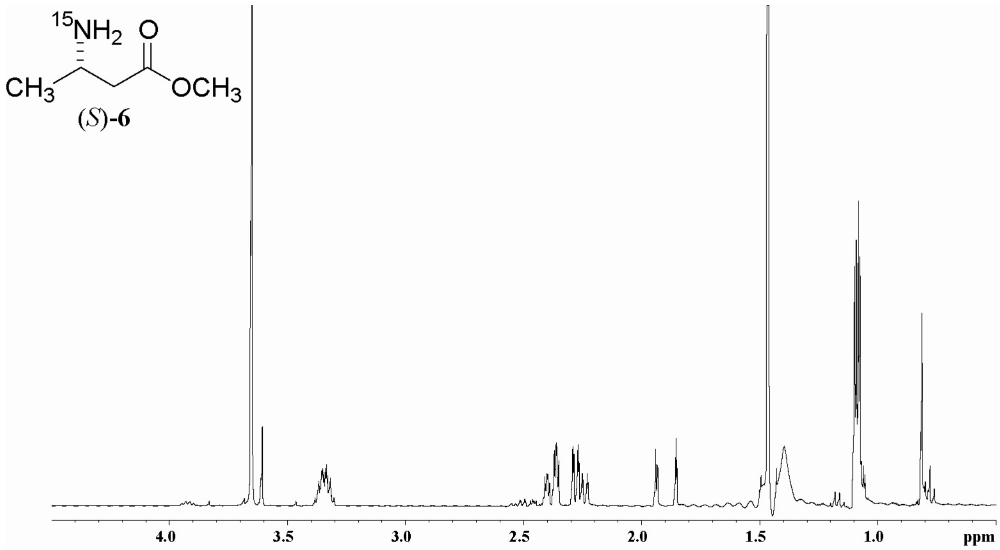

(*S*)-**6**

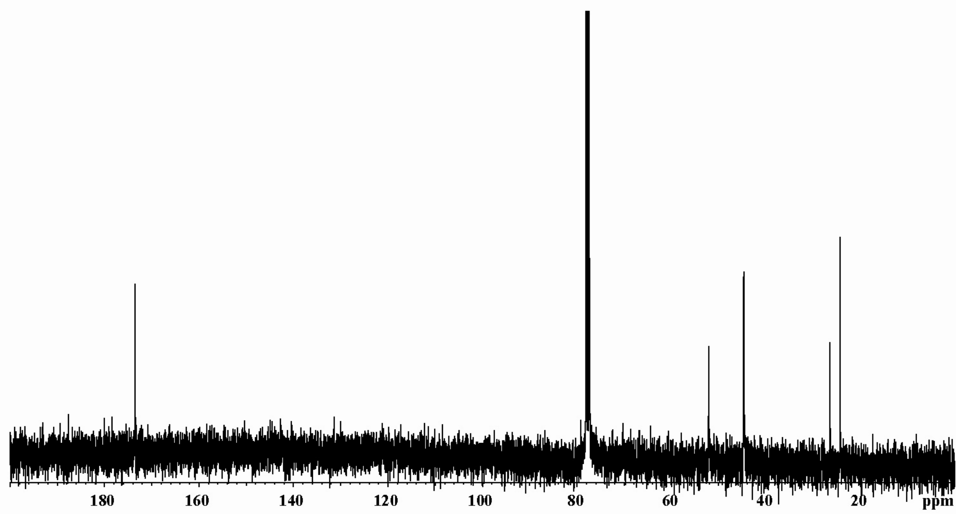

4. ^{1}H NMR (400 MHz, $CDCl_3$): δ 1.09 (dd, J = 2.4, 6.8 Hz, 3H), 1.40 (bs, 2H), 1.46 (C_5H_{10}), 2.26 (ddd, J = 1.5, 8.8, 15.6 Hz, 1H), 2.38 (ddd, J = 3.4, 4.4, 15.6 Hz, 1H), 3.3-3.4 (m, 1H), 3.65 (s, 3H). ^{13}C NMR (100 MHz, $CDCl_3$): δ 24.2, 26.4 (C_5H_{10}), 44.6, 44.7, 52.1, 173.5. (Note: C_5H_{10} is the solvent cyclopentane.)

^{15}N-labeled β-amino esters were synthesized from [^{15}N]alanine via the Arndt-Eistert protocol. (Podlech, J.; Seebach, D. *Liebigs Ann.* **1995**, 1217-1228.)

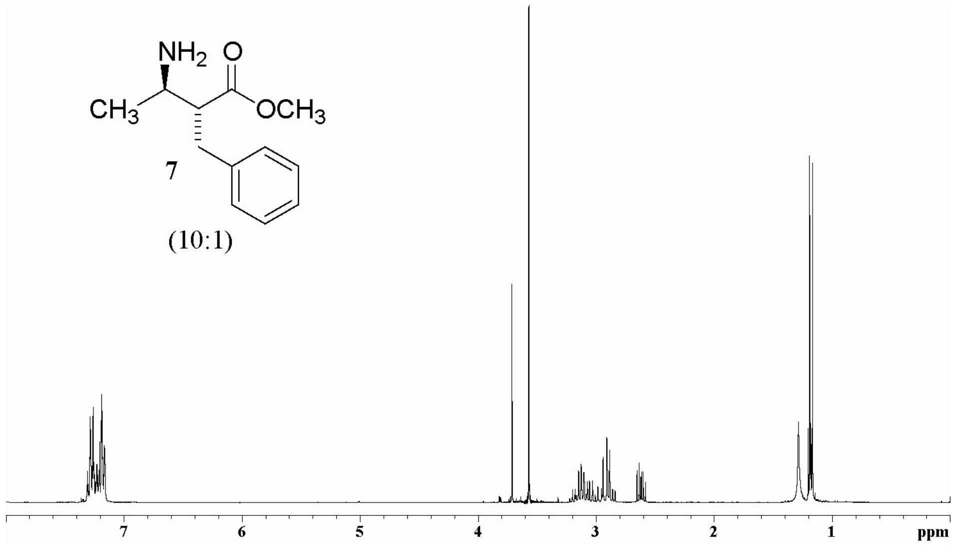

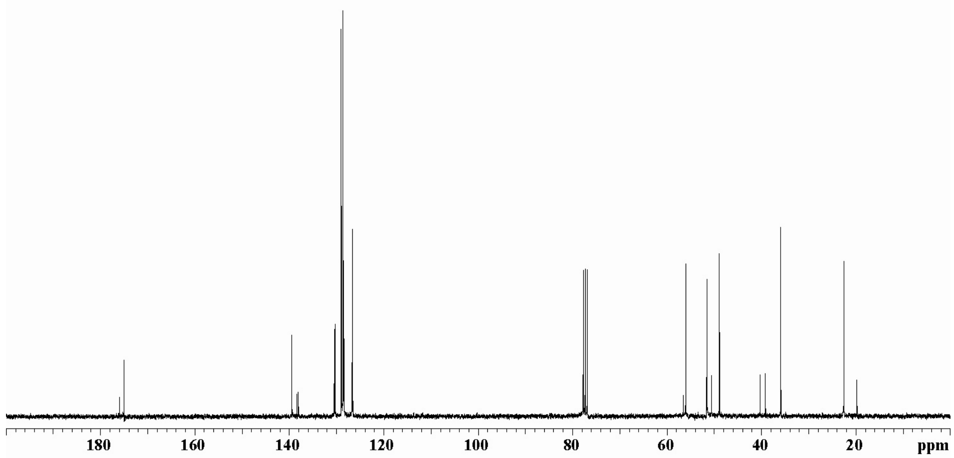

5. ^{1}H NMR (300 MHz, $CDCl_3$): δ 1.18 (d, J = 6.6 Hz, 3H), 1.29 (bs, 2H), 2.62 (dt, J = 5.7, 10.2 Hz, 1H), 2.87 (dd, J = 5.7, 13.5 Hz, 1H), 2.94 (dd, J = 9.3, 13.2 Hz, 1H), 3.13 (m, 1H), 3.57 (s, 3H), 7.13-7.26 (m, 5H). ^{13}C NMR (75 MHz, $CDCl_3$): δ 22.5, 35.8, 48.9, 51.6, 56.0, 126.7, 128.9, 130.5, 139.4, 174.9.

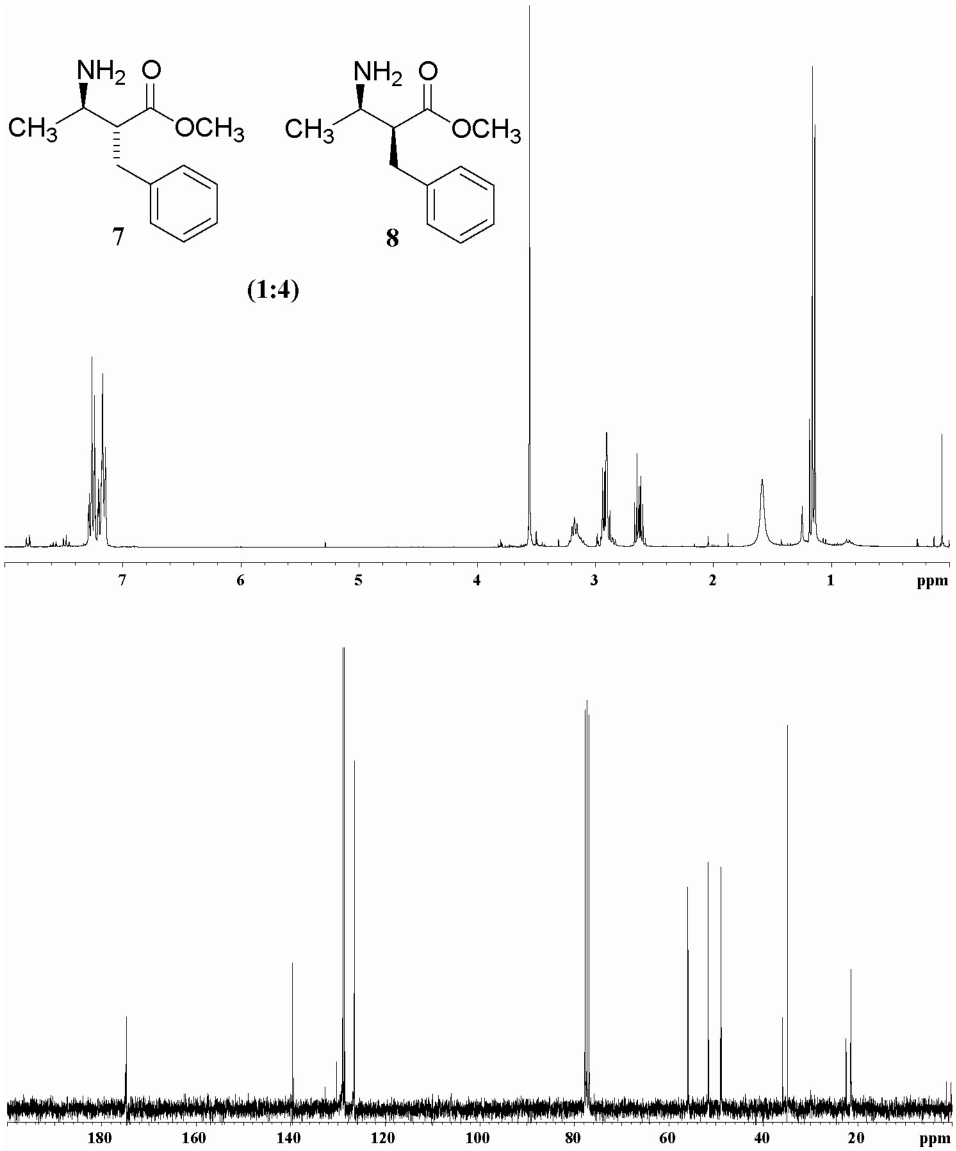

6. **8**: ^{1}H NMR (300 MHz, $CDCl_3$): δ 1.15 (d, J = 6.6 Hz, 3H), 1.59 (bs, 2H), 2.61-2.67 (m, 1H), 2.83-2.98 (m, 2H), 3.10-3.22 (m, 1H), 3.56 (s, 3H), 7.14-7.29 (m, 5H). ^{13}C NMR (75 MHz, $CDCl_3$): δ 21.5, 34.9, 49.0, 51.6, 55.9, 126.5, 128.6, 128.9, 139.6, 174.8. For **7**, see Figure 5 (p S10).

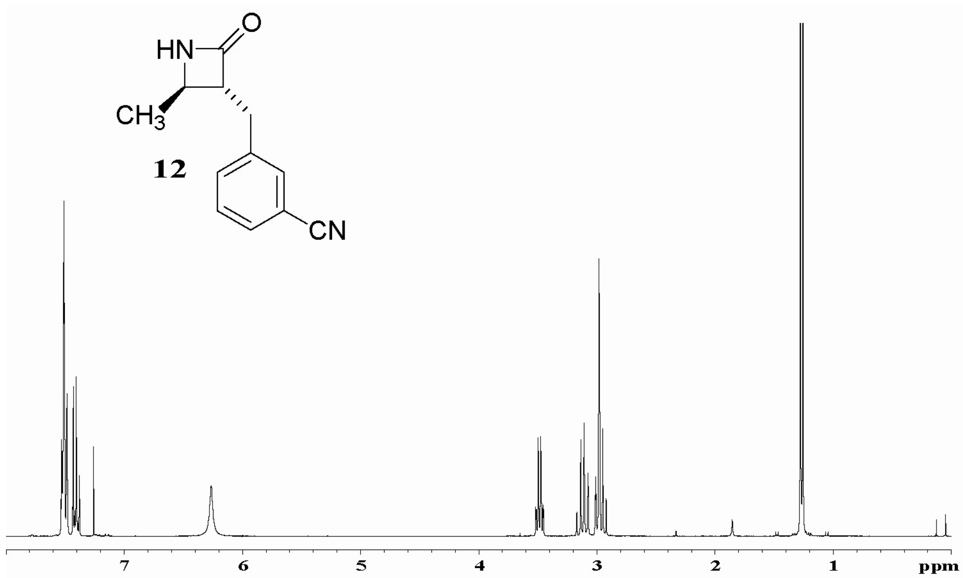

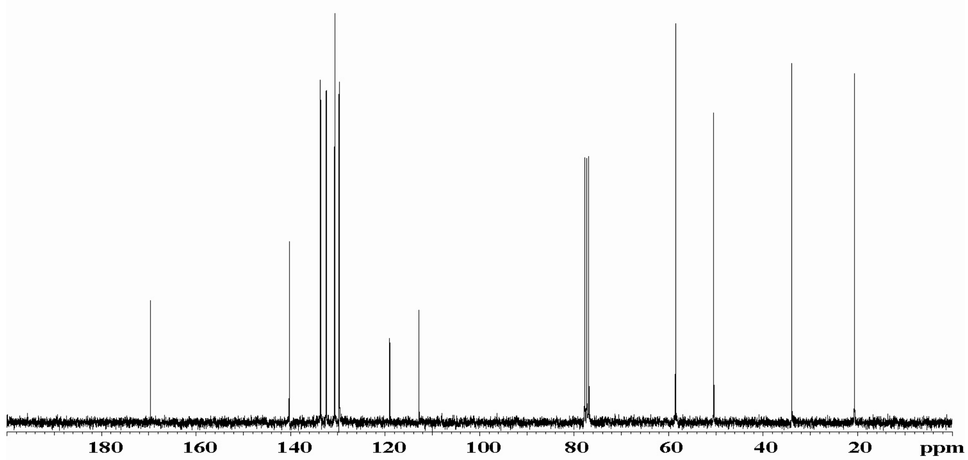

7. ^{1}H NMR (300 MHz, $CDCl_3$): δ 1.26 (d, J = 6 Hz, 3H), 2.98 (m, 2H), 3.12 (m, 1H), 3.48 (dq, J = 1.8, 6 Hz, 1H), 6.26 (bs, 1H), 7.38-7.54 (m, 4H). ^{13}C NMR (75 MHz, $CDCl_3$): δ 20.7, 34.0, 50.5, 58.5, 112.8, 119.0, 129.7, 130.7, 132.4, 133.6, 140.2, 169.6.

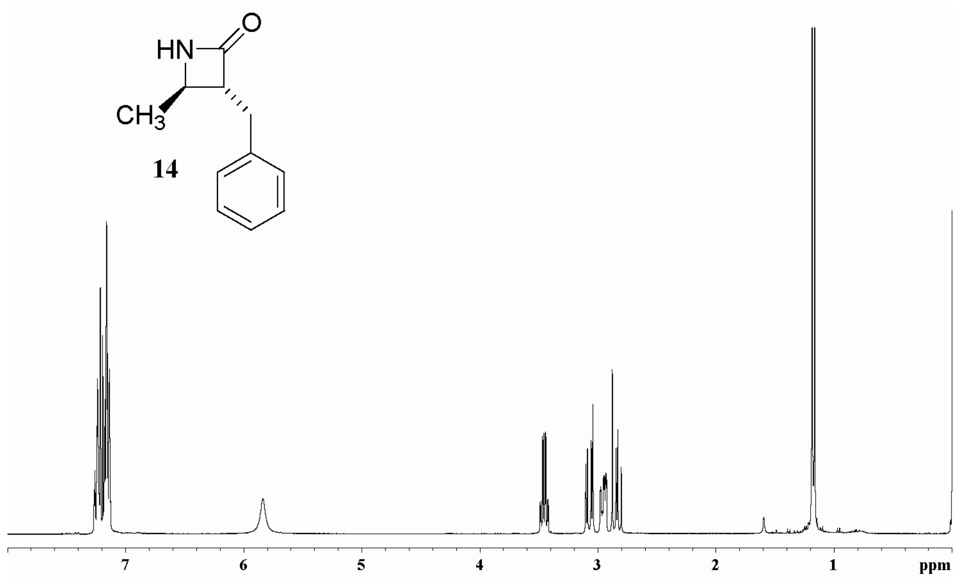

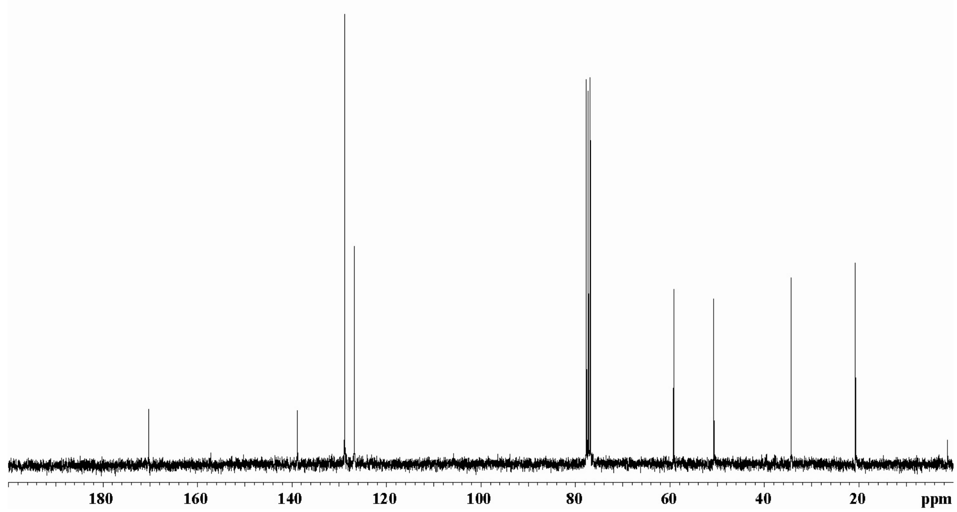

8. ^{1}H NMR (300 MHz, $CDCl_3$): δ 1.17 (d, J = 6 Hz, 3H), 2.84 (dd, J = 9.3, 13.5 Hz, 1H), 2.95 (m, 1H), 3.08 (dd, J = 4.8, 13.5 Hz, 1H), 3.45 (dq, J = 2.1, 6.3 Hz, 1H), 5.84 (bs, 1H), 7.19-7.27 (m, 5H). ^{13}C NMR (75 MHz, $CDCl_3$): δ 20.7, 34.4, 50.7, 59.2, 126.7, 128.8, 128.9, 138.8, 170.4.

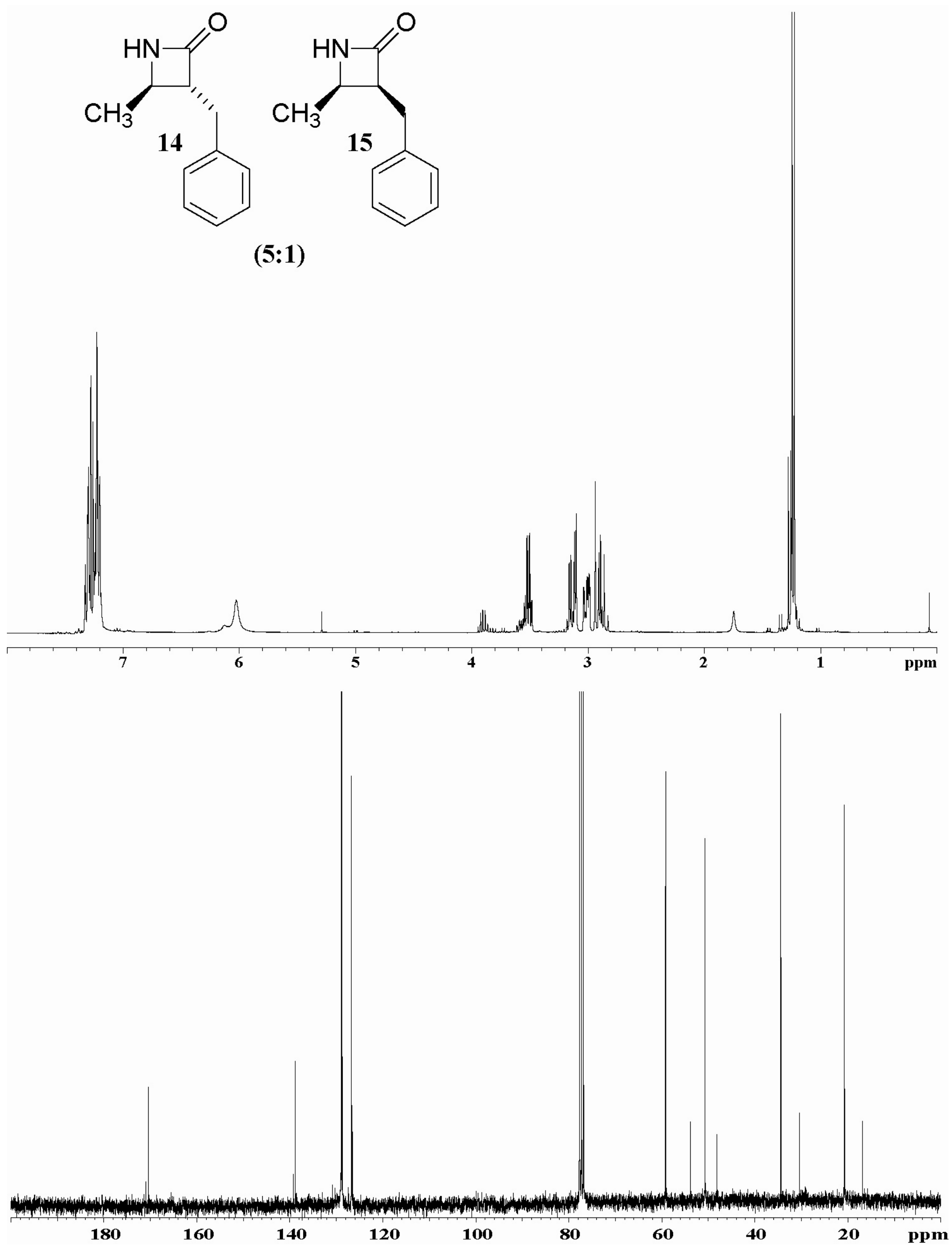

9. **15**: ^{1}H NMR (300 MHz, $CDCl_3$): δ 1.27 (d, J = 6 Hz, 3H), 2.83-2.94 (m, 1H), 3.00-3.04 (m, 1H), 3.10-3.20 (m, 1H), 3.55-3.61 (m, 1H), 6.13 (bs, 1H), 7.18-7.33 (m, 5H). ^{13}C NMR (75 MHz, $CDCl_3$): δ 16.9, 30.4, 48.1, 53.8, 126.6, 128.6, 139.2., 170.9. For **14**, see Figure 8 (pg S13).

Control Experiments

10. LiHMDS-mediated enolization of tosylate salt 2

LiHMDS (0.167 g, 1.0 mmol) was weighed into a 15 mL flask and dissolved in 6.3 mL THF and 2.0 mL toluene. The solution was placed in a ReactIR vessel and cooled to 0 ^{o}C for 20 min. LiHMDS (0.167 g, 1.0 mmol) was weighed into a 5 mL Kimble vial and dissolved in 1.0 mL THF. Tosylate salt **2** (0.289 g, 1.0 mmol) was added to the 5 mL vial with LiHMDS to afford the free base. The mixture was initially heterogeneous (salt **2** is insoluble in THF). After a few seconds, the solution became homogeneous and then immediately a white precipitate formed (LiOTs). This heterogeneous mixture was then injected into the IR vessel containing 1.0 mmol of LiHMDS and the spectrum was recorded within 20 s. The absence of a C=O absorbance indicates complete and instantaneous enolization. The enolate C=C absorbance was at 1620 cm^{-1}.

11. LiHMDS-mediated enolization and cyclization of 4.

LiHMDS (0.167 g, 1.0 mmol) was dissolved in 7.3 mL THF and 2.5 mL toluene. The solution was placed in a ReactIR vessel and cooled to -50 ^{o}C for 20 min. In a separate 5 mL Kimble vial, **4** (0.266 g, 1.1 mmol) was dissolved in 0.87 mL THF and 100 µL was injected into the IR vessel. The spectra were collected every 30 s. The C=O absorbance (1732 cm^{-1}) decreased to the baseline with the appearance of a new absorbance at 1620 cm^{-1}. The pseudo-first-order rate constant was 2.3 ± 0.1 x 10^{-3} s^{-1}. An additional 400 µL of the solution of ester **4** was injected and the reaction was quenched with H_2O when the C=O absorbance had disappeared. Chromatographic separation of the products (95/5 CH_2Cl_2/CH_3OH) provided lactam **14** in 54% yield and esters **4** and **5** in a 19 and 19% yield, respectively.

12. LiHMDS-mediated enolization of 5.

LiHMDS (0.167 g, 1.0 mmol) was dissolved in 7.3 mL THF and 2.5 mL toluene. The solution was placed in a ReactIR vessel and cooled to -50 ^{o}C for 20 min. In a separate 5 mL Kimble vial, ester **5** (0.315 g, 1.1 mmol) was dissolved in 1.05 mL THF and 100 µL was injected into the IR vessel. The spectra were collected every 30 s. The C=O absorbance (1732 cm^{-1}) decreased to the baseline with the appearance of a new absorbance at 1620 cm^{-1}. The pseudo-first-order rate constant was 16 ± 1 x 10^{-3} s^{-1}. An additional 400 µL of the solution of ester **5** was injected and the reaction was quenched with H_2O when the C=O absorbance had disappeared. Chromatographic isolation of the products (95/5 CH_2Cl_2/CH_3OH) provided esters **4** and **5** in a 28 and 56% yield, respectively.

13. LiHMDS-mediated enolization of free base 6.

LiHMDS (0.201 g, 1.2 mmol) was dissolved in 7.4 mL THF and 2.25 mL toluene. The solution was placed in a ReactIR vessel and cooled to 0 °C for 20 min. Ester (*R*)-**6** (0.117 g, 1.0 mmol) was injected into the IR vessel and the spectrum was acquired within 20 s. The absence of a C=O absorbance indicates complete enolization. The enolate C=C absorbance was at 1618 cm^{-1}.

14. LiHMDS-mediated enolization and cyclization of 7/8.

The reaction of LiHMDS with **7** (•) and **8** (▾) is instantaneous in 9.0 M THF/toluene at 0 °C. Therefore, the formation of lactams **14** (▪) and **15** (♦) was monitored by incremental addition of LiHMDS equivalents with subsequent GC analysis post-quenching. The reaction yields a final ratio of lactams **14**:**15** of 7.5:1 using an initial ester **7**:**8** ratio of 1.5:1.

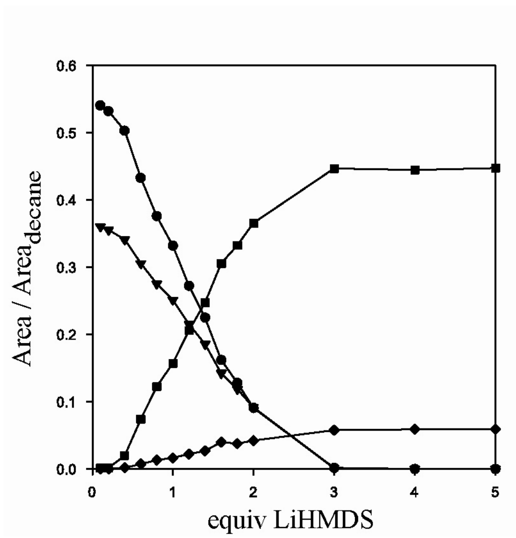

15. In-situ formation of lactam 14 with LiHMDS/*rac*-9.

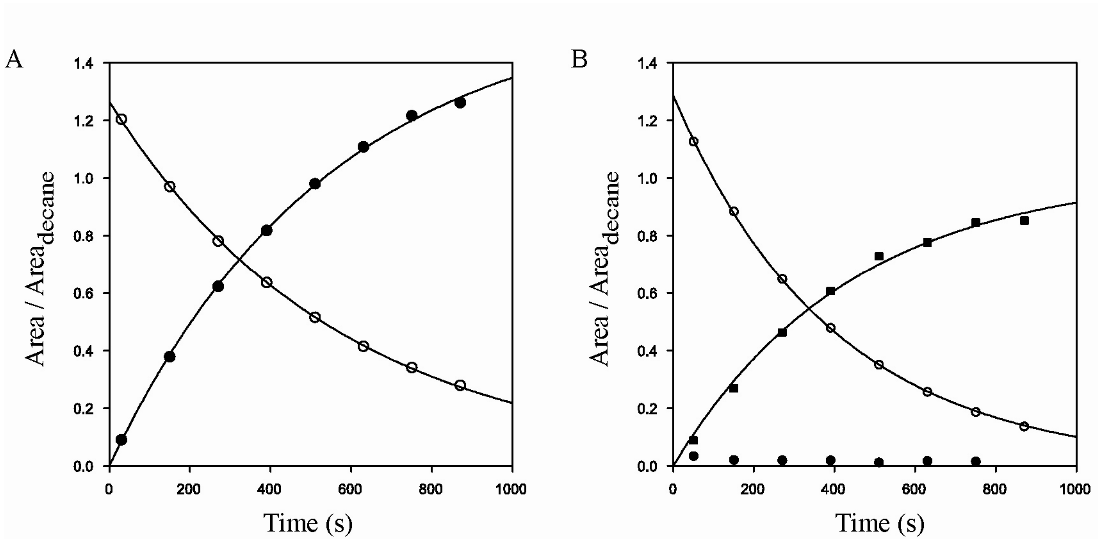

(A) Enolate *rac*-**9** (0.074 g, 0.6 mmol) was dissolved in 1.51 mL THF and 0.42 mL toluene at 0 °C. A stock solution of BnBr (50 μL, 0.2 M BnBr/0.1 M decane in toluene) was injected and the reaction monitored by GC analysis of H_2O-quenched samples (Et_2O extract). The pseudo-first-order rate constant for the loss of BnBr (○) is 1.760 ± 0.001 x 10^{-3} s^{-1} and for the appearance of ester **7** (●) is 1.8 ± 0.1 x 10^{-3} s^{-1}.

(B) Enolate *rac*-**9** (0.074 g, 0.6 mmol) was dissolved in 1.51 mL THF and 0.42 mL toluene at 0 °C. LiHMDS (0.010 g, 0.06 mmol) was added to the vial. A stock solution of BnBr (50 μL, 0.2 M BnBr/0.1 M decane in toluene) was injected and the reaction monitored by GC analysis of H_2O-quenched aliquots (Et_2O extract). The pseudo-first-order rate constant for the loss of BnBr (○) is 2.55 ± 0.02 x 10^{-3} s^{-1} and for the appearance of lactam **14** (■) is 2.3 ± 0.2 x 10^{-3} s^{-1}.

16. Formation of stilbene 13 from LiHMDS/3.

LiHMDS (0.033 g, 0.2 mmol) was weighed into a 5 mL round-bottom flask. THF (1.46 mL) and toluene (0.51 mL) were added to the flask. The solution was cooled to 0 °C for 10 min. A stock solution of **3** (32 μL, 0.6 M **3**/0.3 M decane in toluene) was added to the flask and the reaction was monitored over 5 min via GC analysis of quenched aliquots. The quench consisted of 3 M HCl/2M NaCl in H_2O (0.5 mL) and Et_2O (1.0 mL). The pseudo-first-order rate constant for the reaction of LiHMDS with **3** to produce stilbene **13** was $8 \pm 1 \times 10^{-3}$ s^{-1} (average of two runs).

17. GC analysis of LiHMDS with BnBr.

LiHMDS (0.033 g, 0.2 mmol) was weighed into a 5 mL round-bottom flask. THF (1.46 mL) and toluene (0.51 mL) were added to the flask. The solution was cooled to 0 °C for 10 min. A stock solution of BnBr (32 μL, 0.6 M BnBr/0.3 M decane in toluene) was added to the flask and the reaction was monitored over 1 h via GC analysis of quenched aliquots. The quench consisted of 3 M HCl/2M NaCl in H_2O (0.5 mL) and Et_2O (1.0 mL). There was no change in the GC area ratio of BnBr/decane over 1 h.

18. Table of k_{rel} for alkylations.

Ester	Electrophile	k_{obsd} (s^{-1})	k_{rel}
(*R*)-**6**	BnBr[a]	$1.75 \pm 0.3 \times 10^{-3}$	2.2
rac-**6**	BnBr[a]	$1.02 \pm 0.3 \times 10^{-3}$	1.3
2	BnBr[b]	$0.8 \pm 0.1 \times 10^{-3}$	1.0
(*R*)-**6**	**3**[a]	$14.6 \pm 0.6 \times 10^{-3}$	18.7
rac-**6**	**3**[a]	$8.3 \pm 0.0 \times 10^{-3}$	10.4
2	**3**[b]	$9.2 \pm 0.1 \times 10^{-3}$	11.5

[a.] 9.0 M THF/toluene, 0.10 M LiHMDS, 0.12 M ester **6**, and 0.01 M electrophile.

[b.] 9.0 M THF/toluene, 0.20 M LiHMDS, 0.11 M salt **2**, and 0.01 M electrophile.

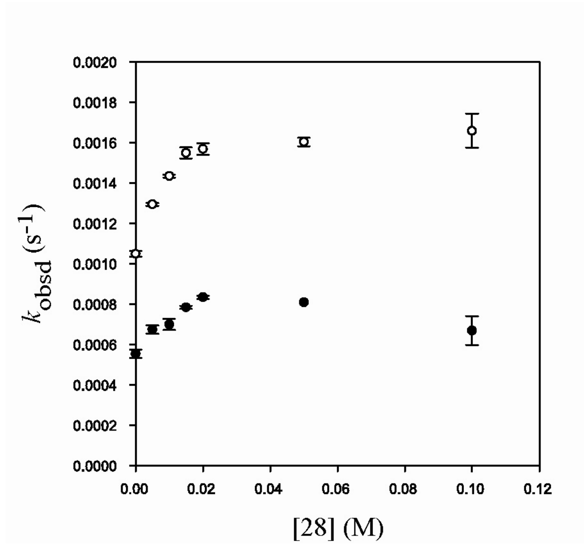

19. Plot of k_{obsd} versus [**28**] in 6.0 M THF/toluene for the alkylation of (*R*)-**9** (○, 0.10 M) and *rac*-**9** (●, 0.10 M) with BnBr (0.01 M) at 0 °C.

20. Table of data for plot in Figure 19.

[**28**] (M)	(*R*)-**9** k_{obsd} (s^{-1})	*rac*-**9** k_{obsd} (s^{-1})
0	$10.5 \pm 0.1 \times 10^{-4}$	$5.5 \pm 0.2 \times 10^{-4}$
0.005	$13.0 \pm 0.1 \times 10^{-4}$	$6.8 \pm 0.2 \times 10^{-4}$
0.01	$14.4 \pm 0.1 \times 10^{-4}$	$7.0 \pm 0.3 \times 10^{-4}$
0.015	$15.5 \pm 0.3 \times 10^{-4}$	$7.8 \pm 0.1 \times 10^{-4}$
0.02	$15.7 \pm 0.3 \times 10^{-4}$	$8.4 \pm 0.1 \times 10^{-4}$
0.05	$16.1 \pm 0.2 \times 10^{-4}$	$8.1 \pm 0.0 \times 10^{-4}$
0.10	$16.6 \pm 0.8 \times 10^{-4}$	$6.7 \pm 0.7 \times 10^{-4}$

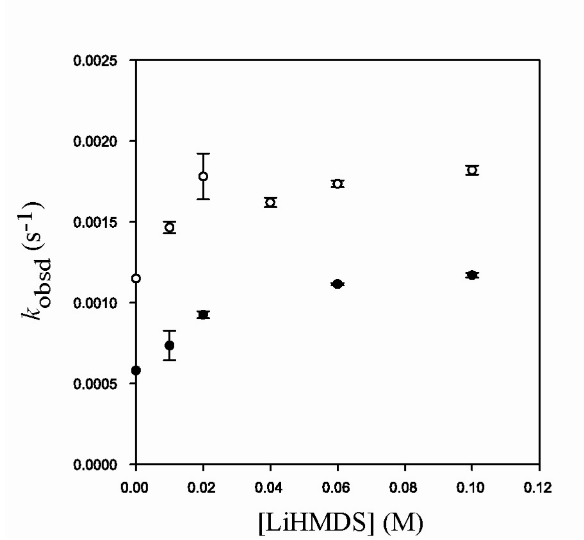

21. Plot of k_{obsd} versus [LiHMDS] in 6.0 M THF/toluene for the alkylation of (*R*)-**9** (○, 0.10 M) and *rac*-**9** (●, 0.10 M) with BnBr (0.01 M) at 0 °C.

22. Table of data for plot in Figure 21.

[LiHMDS] (M)	(*R*)-**9** k_{obsd} (s^{-1})	*rac*-**9** k_{obsd} (s^{-1})
0.09	$10.7 \pm 0.1 \times 10^{-4}$	$5.5 \pm 0.3 \times 10^{-4}$
0.10	$11.5 \pm 0.0 \times 10^{-4}$	$5.8 \pm 0.0 \times 10^{-4}$
0.11	$14.7 \pm 0.4 \times 10^{-4}$	$7.4 \pm 0.9 \times 10^{-4}$
0.12	$18 \pm 1 \times 10^{-4}$	$9.2 \pm 0.2 \times 10^{-4}$
0.16	$16.2 \pm 0.3 \times 10^{-4}$	$11.2 \pm 0.1 \times 10^{-4}$
0.20	$18.2 \pm 0.3 \times 10^{-4}$	$11.7 \pm 0.1 \times 10^{-4}$

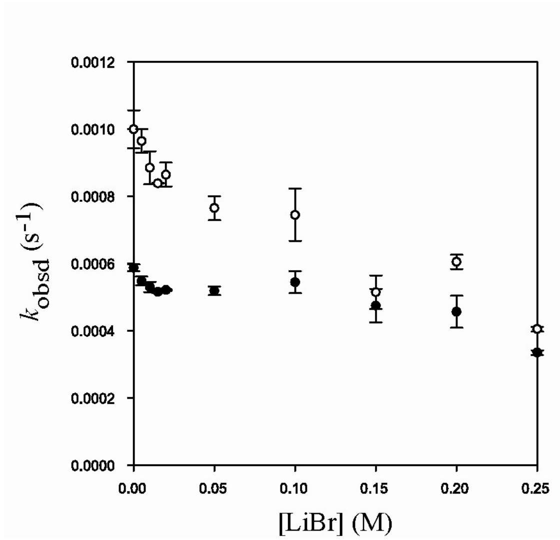

23. Plot of k_{obsd} versus [LiBr] in 6.0 M THF/toluene for the alkylation of (*R*)-**9** (○, 0.10 M) and *rac*-**9** (●, 0.10 M), respectively, with BnBr (0.01 M) at 0 °C.

24. Table of data for plot in Figure 23.

[LiBr] (M)	(*R*)-**9** k_{obsd} (s^{-1})	*rac*-**9** k_{obsd} (s^{-1})
0.00	$10.0 \pm 0.5 \times 10^{-4}$	$5.9 \pm 0.1 \times 10^{-4}$
0.005	$9.6 \pm 0.4 \times 10^{-4}$	$5.5 \pm 0.1 \times 10^{-4}$
0.01	$8.8 \pm 0.5 \times 10^{-4}$	$5.3 \pm 0.1 \times 10^{-4}$
0.015	$8.39 \pm 0.01 \times 10^{-4}$	$5.12 \pm 0.03 \times 10^{-4}$
0.02	$8.6 \pm 0.4 \times 10^{-4}$	$5.22 \pm 0.02 \times 10^{-4}$
0.05	$7.6 \pm 0.4 \times 10^{-4}$	$5.2 \pm 0.1 \times 10^{-4}$
0.10	$7.4 \pm 0.8 \times 10^{-4}$	$5.5 \pm 0.3 \times 10^{-4}$
0.15	$5.2 \pm 0.5 \times 10^{-4}$	$4.8 \pm 0.5 \times 10^{-4}$
0.20	$6.0 \pm 0.2 \times 10^{-4}$	$4.6 \pm 0.5 \times 10^{-4}$
0.25	$4.05 \pm 0.07 \times 10^{-4}$	$3.35 \pm 0.07 \times 10^{-4}$

Single-Crystal X-ray Structure Data

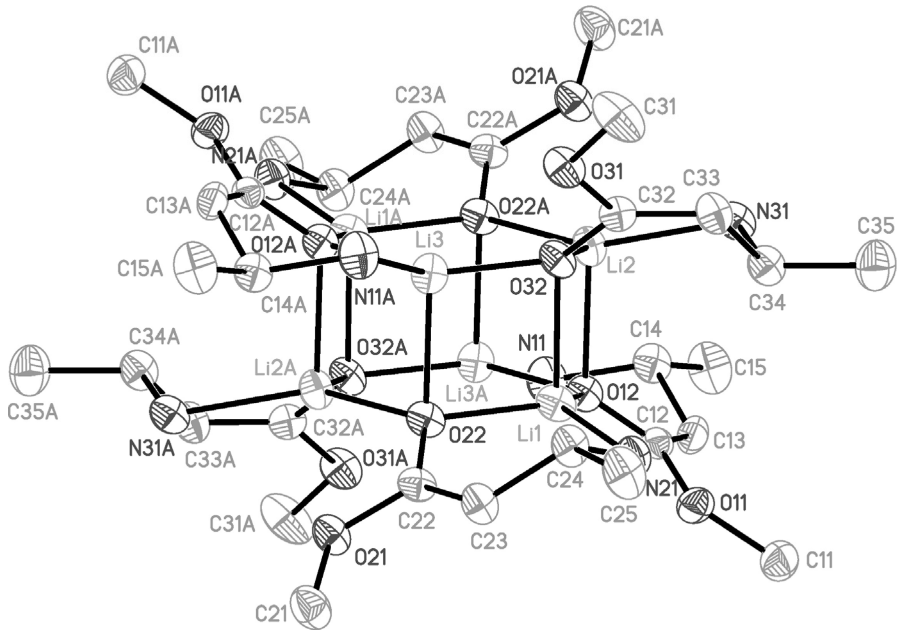

25. Crystals of *rac*-**9** were obtained from a 0.20 M enolate solution in 9.0 M THF/toluene held at -20 °C over 24 h. Single crystals suitable for X-ray diffraction were coated with polyisobutylene oil in a glovebox and were quickly transferred to the goniometer head of a Siemens SMART (λ = 0.71073 A T=173 K). The crystal belongs to the space group P1(bar). 1818 frames were collected using 0.3 deg. omega scans ($2\theta_{max}$ = 46.52 º). The data were processed with Bruker SAINT and SADABS programs to yield a total of 6120 unique reflections (R(int)=0.0575). The structure was solved using direct method (SHELXS) completed by subsequent Fourier synthesis and refined by full-matrix least-squares procedures (SHELXL). At final convergence, R(1) = 0.0665 for 3433 Fo > 4sig(Fo) and GOF = 0.949 for 772 parameters. For the crystal structure data and refinement details, see McNeil, A. J.; Toombes, G. E. S.; Chandramouli, S. V.; Vanasse, B. J.; Ayers, T. A.; O'Brien, M. K.; Lobkovsky, E.; Gruner, S. M.; Marohn, J. A.; Collum, D. B. *J. Am. Chem. Soc.* **2004**, *126*, 5938-5939 (CCDC 231371).

Powder Diffraction Data

26. Powder X-ray diffraction data was collected on a Scintag XDS-2000 with Cu K_α radiation and a liquid nitrogen cooled Ge solid-state detector. The sample was packed inside a glove box under argon atmosphere in a holder for air-sensitive samples to protect it from atmospheric moisture. The pattern was measured over the angular range 2 to 50° 2θ at a rate of 0.1°/min. The data were fitted with the Le Bail method, using lattice constants from single crystal data as a starting point. The lattice constants refined to values of a = 13.7655 Å, b = 13.2951 Å, c = 13.8038 Å, α = 11.765°, β = 92.50° and γ = 103.72°. (For reference, see Le Bail, A.; Duroy, H.; Fourquet, J. L. *Mater. Res. Bull*. **1988**, *23*, 447-452 and Rodriguez-Carvajal, J. FULLPROF: A Program for Rietveld Refinement and Pattern Matching Analysis. *Abstracts of the Satellite Meeting on Powder Diffraction of the XVth Congress of the IUCr*, Toulouse, France, 1990; p 127.)

27. Powder diffraction pattern for *rac*-**9** and the comparison of calculated fit to the data is shown.

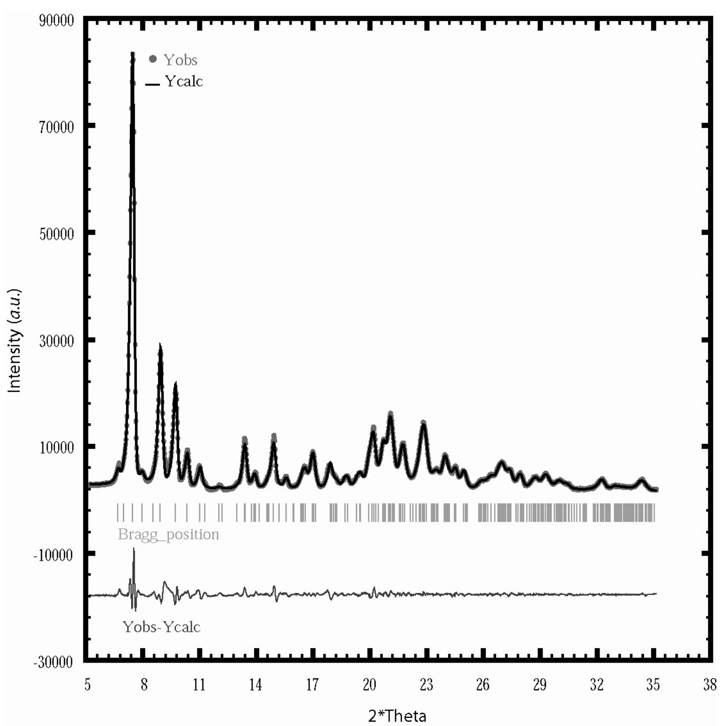

Small-Angle X-ray Scattering Data

28. Experimental Details. Small angle X-ray scattering (SAXS) data were obtained using an RU-H3R Cu rotating anode X-ray generator directed through a nickel filter and collimated with orthogonal Franks mirrors (d_{max} = 400 Å). Tantalum slits at the sample stage trim the beam to approximately 1 mm x 1 mm with an average flux of 4 x 10^7 X-rays per second. Sample temperature was monitored with a 100Ω platinum RTD sensor and regulated with a water-cooled Peltier controller operating within the vacuum beam path. Sample temperature was maintained at 0 °C. Scattering path lengths from 10 cm to 100 cm were used to measure a wide range of sizes. Diffraction patterns were recorded (multiple exposures integrated to give 1-2 hours of total time) with a home-built CCD detector. The detector-sample distance was calibrated with powder patterns of silver stearate and silver behenate. Samples were flame-sealed in 1 mm glass X-ray capillary.

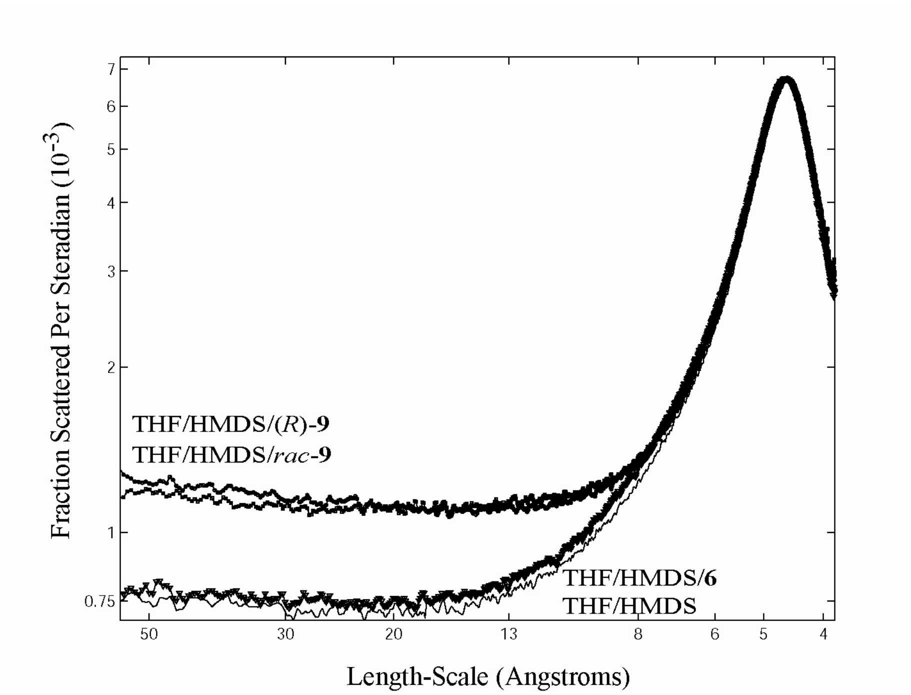

29. Plot of the scattering intensity (I) as a function of momentum transfer (s). Typical concentrations were 12 M THF, 0.5 M HMDS, and 0.5 M **6** or **9**. The THF contributes a strong peak at 4.56 ± 0.25 Å corresponding to the mean THF-THF distance in solution. When the enolate is added to the solution, extra scattering occurs at longer length-scales giving clear indication that the enolate forms assemblies that are measurably larger than the monomer (**6**). No new features were observed for length-scales longer than 50 Å.

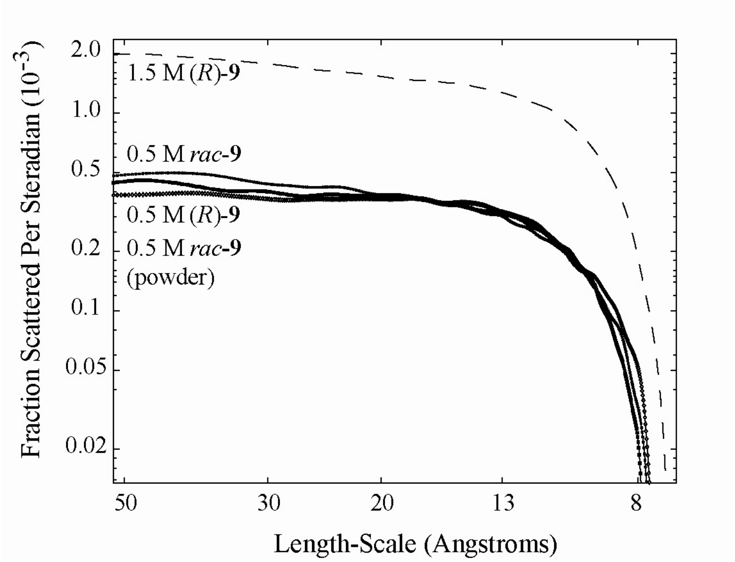

30. Plot of the additional scattering as a function of momentum transfer. Solvation effects make it difficult to unambiguously determine the size of the scattering objects. However, the objects should be between 7 and 14 Å, as this is the length over which the scattering changes markedly. The crystal structure of the hexamer allows us to compute its size in solution. In vacuum, the diameter is 8.88 Å, but the apparent diameter can vary from 6.5 and 13.1 Å depending on how the hexamer is solvated. Although the observed scattering is not that of ideal, isolated particles in solution, the apparent length-scale is consistent with a solution of hexamers.

Solubility Studies Using In-Situ IR

31. Calibration plot. Using 2,2,4,4-tetramethyl-3-pentanone as an internal standard (C=O, 1684 cm^{-1}), a calibration plot to determine [enolate] based on the ratio of absorbance (enolate) / absorbance (standard) was constructed in 9.0 M THF/toluene at 0 ^{o}C. The line depicts an unweighted least-squares fit to $[Abs_{rac\text{-}\mathbf{9}}/Abs_{standard}] = m[rac\text{-}\mathbf{9}] + [Abs_{rac\text{-}\mathbf{9}}/Abs_{standard}]_o$ with m = 23.1 ± 0.8 and $[Abs_{rac\text{-}\mathbf{9}}/Abs_{standard}]_o$ = 0.4 ± 0.1.

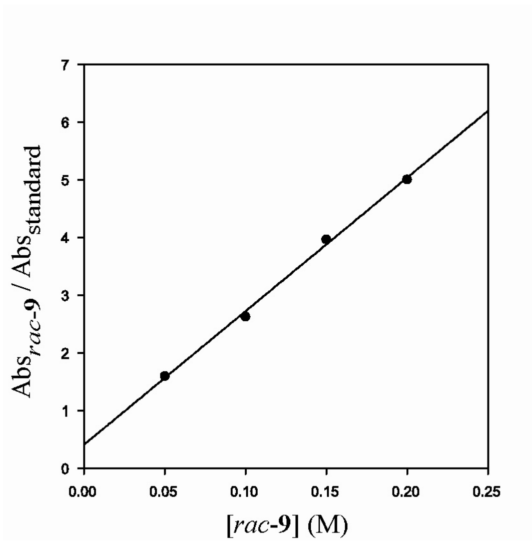

32. Supersaturation. Supersaturated solutions of *rac*-**9** in 9.0 M THF/toluene were monitored via in situ IR at 0 °C until equilibrium was reached. A representative example is described in more detail as follows: A solution of 0.87 M LiHMDS in 9.0 M THF/toluene was placed in the IR vessel and cooled to 0 °C for 20 min. The baseline spectrum was acquired and the reaction started. Injecting 1.0 g of **6** into the IR vessel produced a 0.85 M solution of *rac*-**9** with complete enolization (1620 cm^{-1}, C=C). The decrease of the C=C absorbance over time was monitored until equilibrium was maintained. 2,2,4,4-tetramethyl-3-pentanone (100 µL) was injected. The final absorbances (*rac*-$\mathbf{9}_{C=C}$, 2,2,4,4-tetramethyl 3-pentanone$_{C=O}$) were recorded and the ratio was compared to the calibration plot to give a solution enolate concentration of 0.22 M.

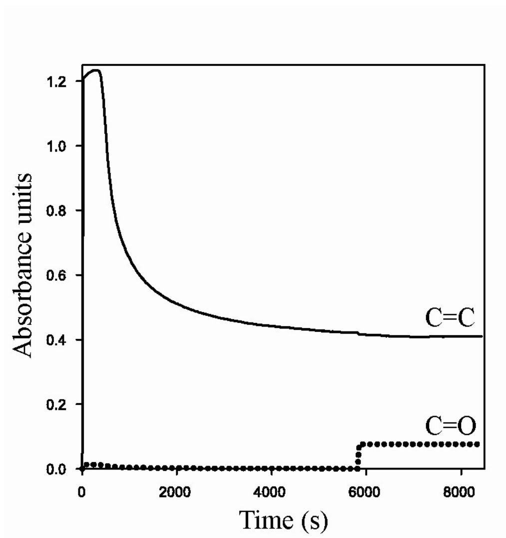

In a separate set of experiments, the absorbances for known concentrations of *rac*-**9** were measured. The solubility was confirmed to be 0.22 M through these studies as well.

Conversely, a 0.85 M solution of (*R*)-**9** was stable in 9.0 M THF/toluene at 0 °C for 7.5 h.

33. Variable-temperature studies. To further probe the solubility of *rac*-**9**, a variable-temperature IR study was undertaken. A representative example is described in more detail as follows: A solution of 0.57 M LiHMDS in 9.0 M THF/toluene was placed in the IR vessel and cooled to 0 °C for 20 min. The baseline spectrum was acquired and the reaction started. Injecting 0.64 g of **6** into the IR vessel produced a 0.55 M solution of *rac*-**9** with complete enolization (1620 cm^{-1}, C=C). 2,2,4,4-tetramethyl-3-pentanone (100 µL) was injected. After 15 min, the bath temperature was lowered to -78 °C and a milky-white precipitate formed with a subsequent decrease in the C=C intensity. After 20 min, the bath temperature was raised to 0 °C and the precipitate re-dissolved indicating the low-temperature precipitate is a different polymorph than the precipitate obtained at 0 °C. Within 2 h at 0 °C, the enolate had again precipitated and equilibrium was established. From the ratio of absorbances at equilibrium, the solubility limit of *rac*-**9** was determined to be 0.20 M in 9.0 M THF/toluene at 0 °C.

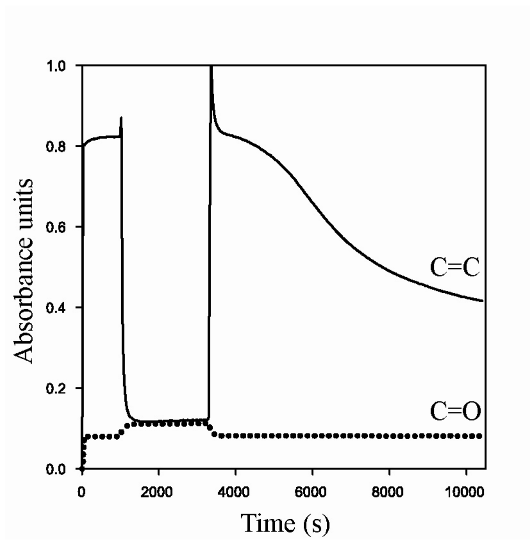

34. Isolation of solid *rac*-9. LiHMDS (1.21 g, 7.2 mmol) was dissolved in THF (7.9 mL) and cooled to 0 °C. Ester *rac*-**6** (0.82 g, 7.0 mmol) was added drop wise to produce solution of *rac*-**9**. Within a few minutes, a milky-white precipitate was evident. The heterogeneous mixture was stirred for 4 h at 0 °C to establish equilibrium. After centrifugation at 0 °C, the supernatant was removed via syringe (6.5 mL) and discarded. The remaining THF was removed under full vacuum at 0 °C. The resulting powder was weighed in a glove box to yield 0.62 g of *rac*-**9** (70% yield). Assuming quantitative enolization of **6** to *rac*-**9**, a 70% isolated yield of solid enolate corresponds to solution [*rac*-**9**] of 0.19 M in the supernatant.

^{6}Li NMR Spectroscopic Studies

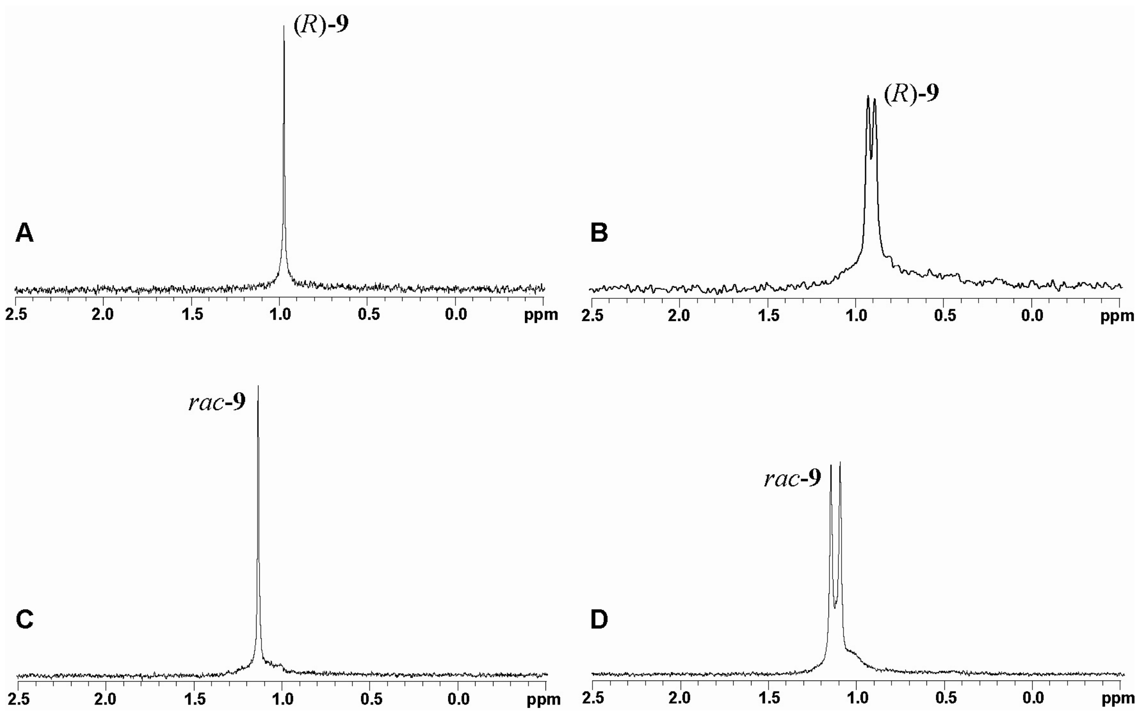

35. ^{6}Li NMR spectra recorded in 9.8 M THF/cyclopentane at -90 ^{o}C: (A) [^{6}Li](*R*)-**9** (0.07 M); (B) [^{6}Li,^{15}N](*S*)-**9** (0.13 M); (C) [^{6}Li]*rac*-**9** (0.13 M); (D) [^{6}Li,^{15}N]*rac*-**9** (0.33 M).

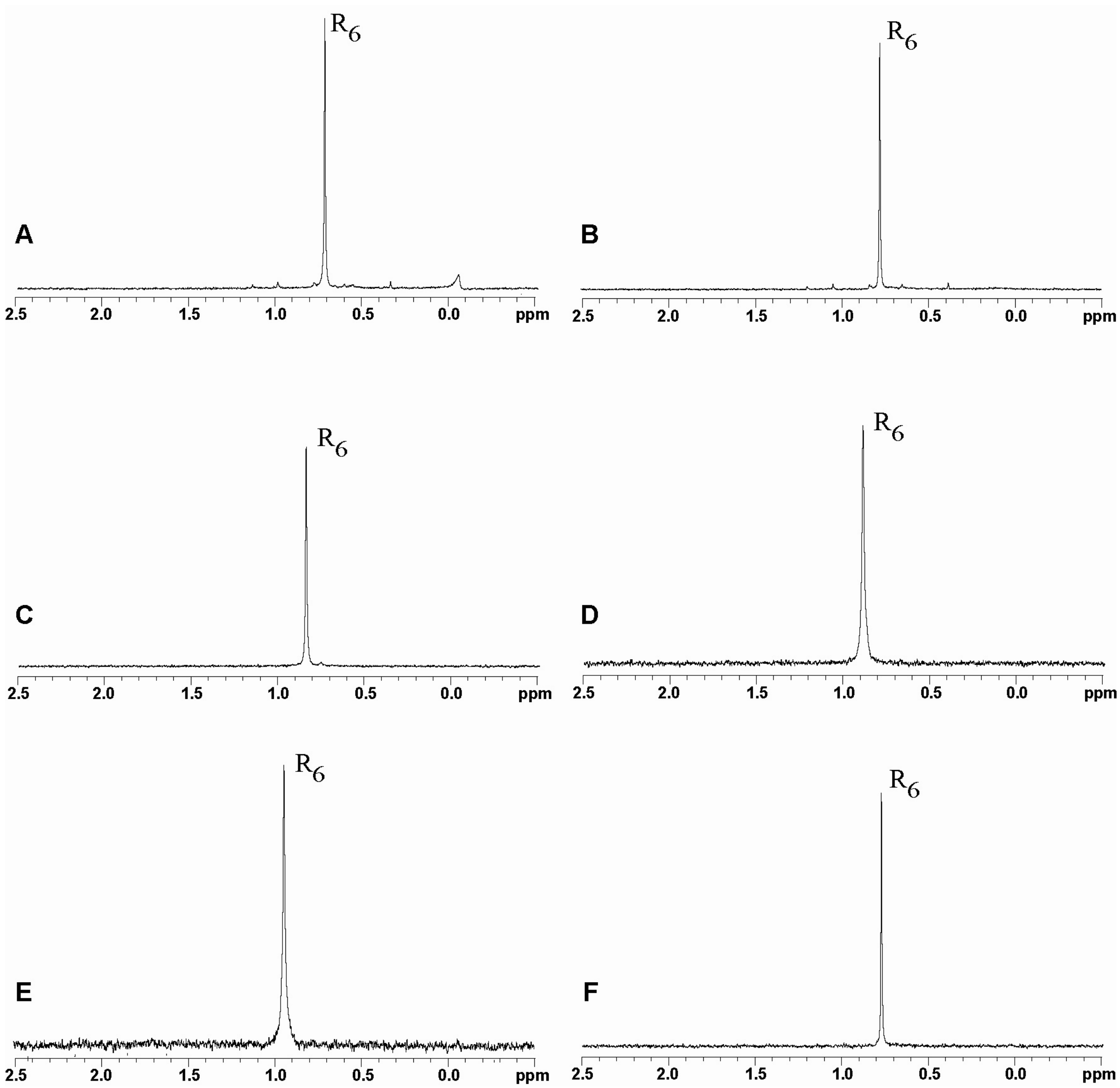

36. ^{6}Li NMR spectra recorded on [^{6}Li](*R*)-**9** (0.20 M) in 9.0 M THF/toluene: (A) -100 °C; (B) -75 °C; (C) -50 °C; (D) -25 °C; (E) 0 °C; (F) -90 °C after temperature series.

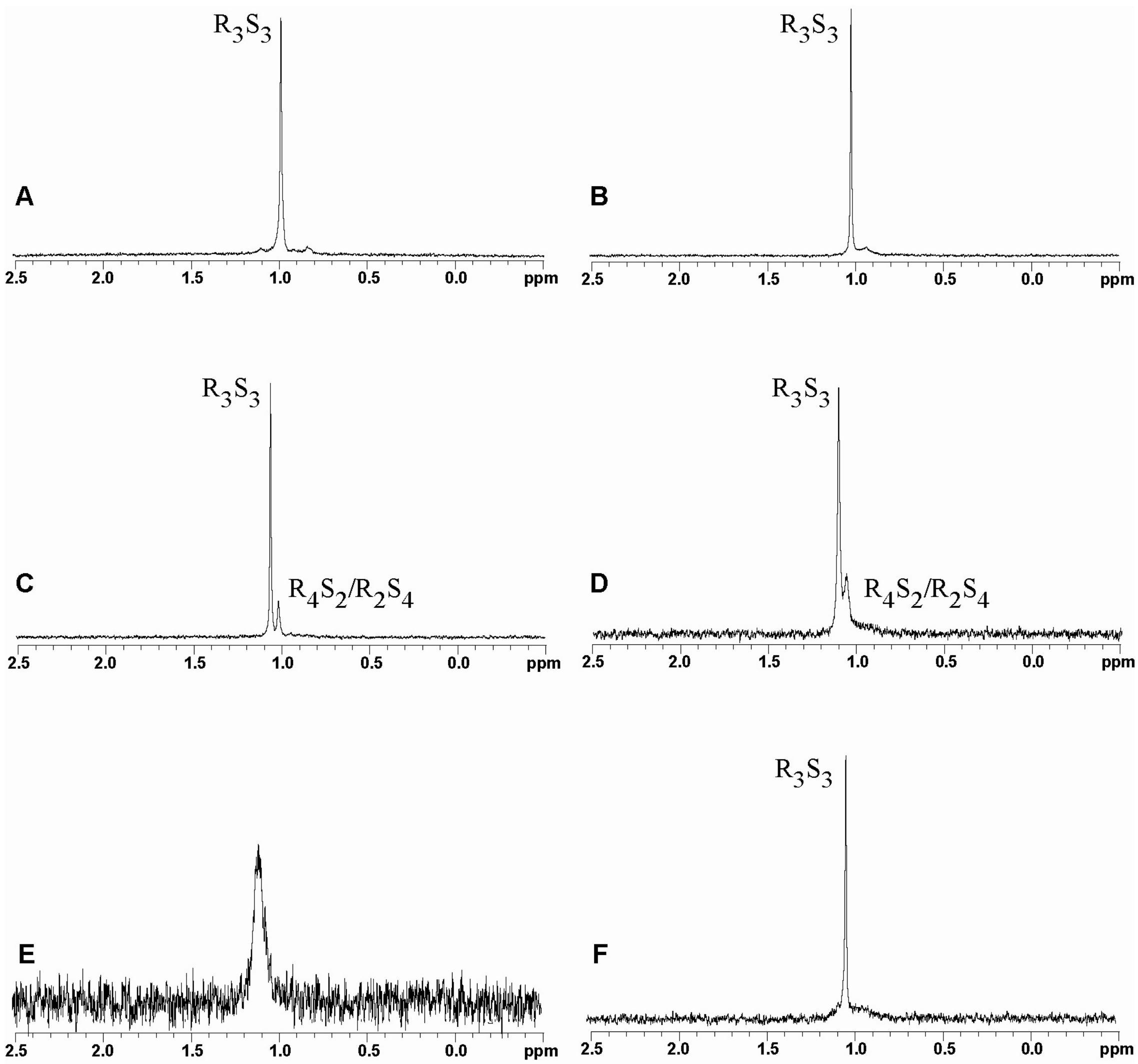

37. ^{6}Li NMR spectra recorded on [^{6}Li]*rac*-**9** (0.20 M) in 9.0 M THF/toluene: (A) -100 °C; (B) -75 °C; (C) -50 °C; (D) -25 °C; (E) 0 °C; (F) -90 °C after temperature series. $\mathbf{R_nS_{N-n}/R_{N-n}S_n}$ and $\mathbf{R_N/S_N}$ refer to pairs of spectroscopically indistinguishable enantiomers.

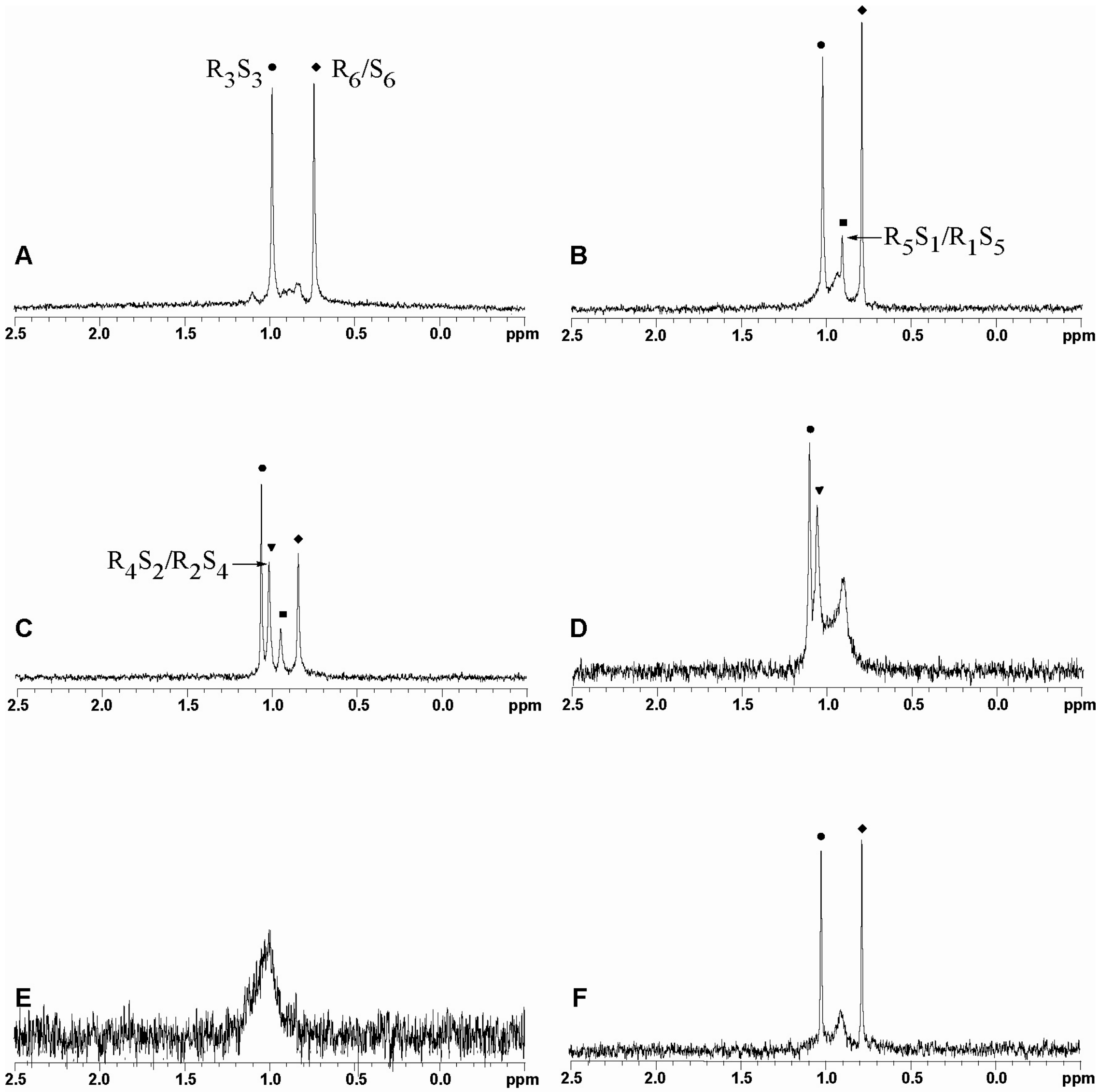

38. ^{6}Li NMR spectra recorded on a mixture of [^{6}Li](*R*)-**9** and [^{6}Li]*rac*-**9** (50% ee) in 9.0 M THF/toluene: (A) -100 °C; (B) -75 °C; (C) -50 °C; (D) -25 °C; (E) 0 °C; (F) -90 °C after temperature series. **R_3S_3** (●); **R_4S_2/R_2S_4** (▾); **R_5S_1/R_1S_5** (■); **R_6/S_6** (◆). **R_nS_{N-n}/$R_{N-n}S_n$** and **R_N/S_N** refer to pairs of spectroscopically indistinguishable enantiomers.

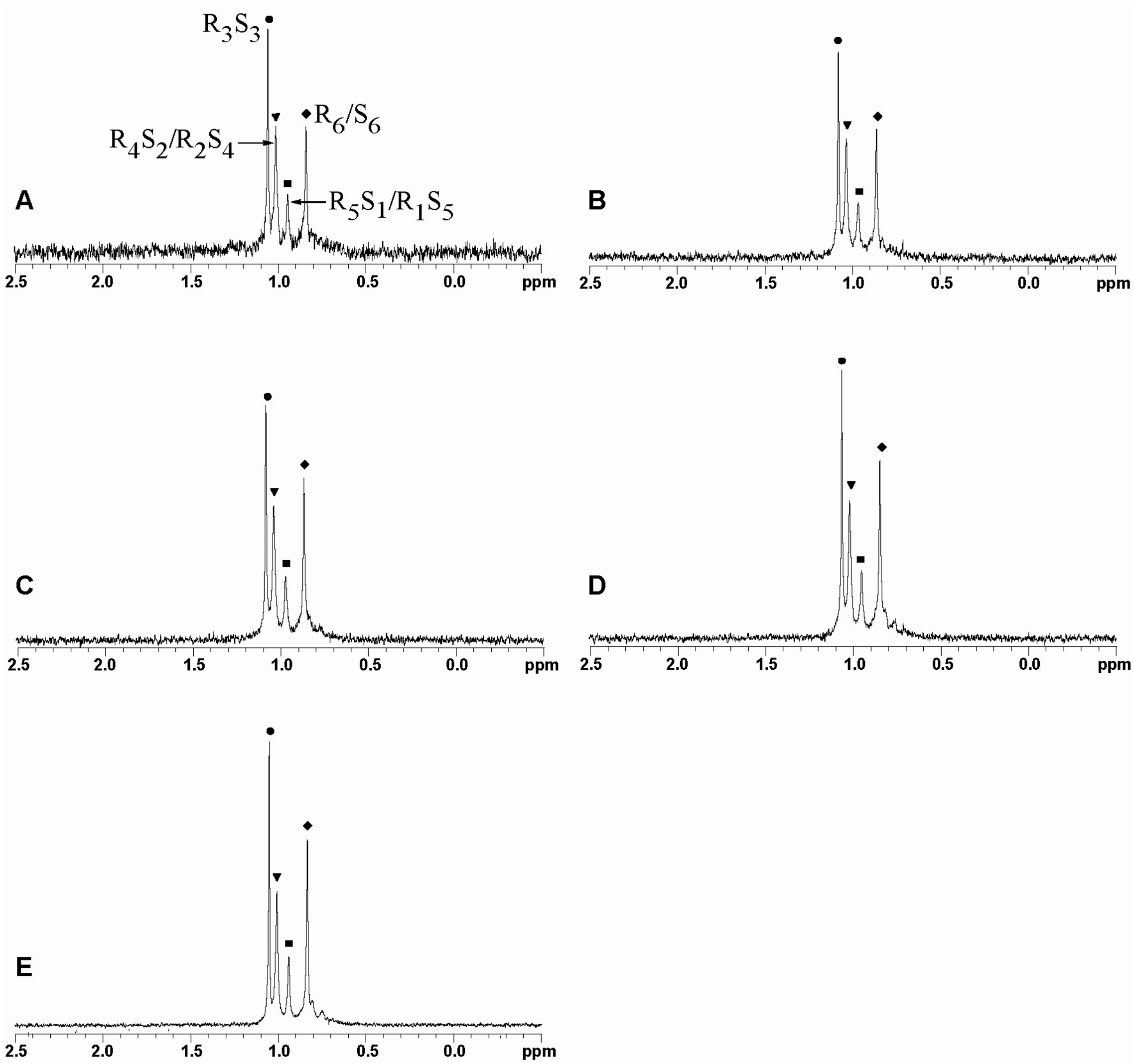

39. ^{6}Li NMR spectra recorded on a mixture of [^{6}Li](*R*)-**9** and [^{6}Li]*rac*-**9** (50% ee) in 9.0 M THF/toluene at -50 °C at various enolate concentrations: (A) 0.04 M; (B) 0.10 M; (C) 0.15 M; (D) 0.25 M; (E) 0.40 M. $\mathbf{R_3S_3}$ (●); $\mathbf{R_4S_2/R_2S_4}$ (▾); $\mathbf{R_5S_1/R_1S_5}$ (▪); $\mathbf{R_6/S_6}$ (◆). $\mathbf{R_nS_{N-n}/R_{N-n}S_n}$ and $\mathbf{R_N/S_N}$ refer to pairs of spectroscopically indistinguishable enantiomers.

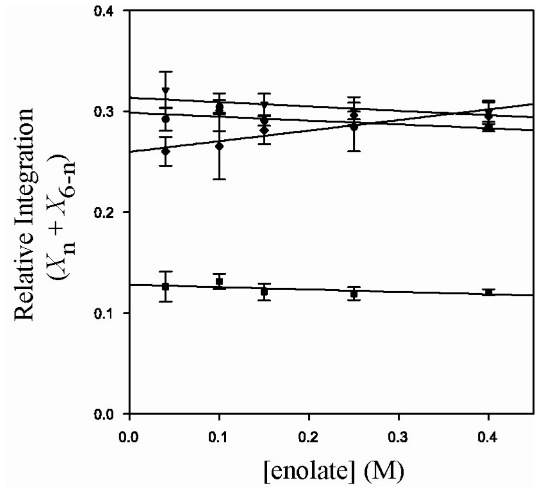

40. Plot of the mole fraction of the aggregate ($X_n + X_{6-n}$) versus [enolate] for the spectra in Figure 39. For the case where n = 3, only X_3 is plotted. **R_3S_3** (●); **R_4S_2/R_2S_4** (▾); **R_5S_1/R_1S_5** (■); **R_6/S_6** (◆). **R_nS_{N-n}/$R_{N-n}S_n$** and **R_N/S_N** refer to pairs of spectroscopically indistinguishable enantiomers.

41. Table of data for the plot in Figure 40. ([^{6}Li](*R*)-**9** and [^{6}Li]*rac*-**9** (50% ee) in 9.0 M THF/toluene at -50 °C.)

[enolate] (M)	**R_3S_3**	**R_4S_2/R_2S_4**	**R_5S_1/R_1S_5**	**R_6/S_6**
0.04	0.29 ± 0.01	0.32 ± 0.02	0.13 ± 0.01	0.26 ± 0.01
0.10	0.30 ± 0.01	0.30 ± 0.02	0.13 ± 0.01	0.27 ± 0.03
0.15	0.29 ± 0.01	0.31 ± 0.01	0.12 ± 0.01	0.28 ± 0.01
0.25	0.28 ± 0.02	0.30 ± 0.01	0.12 ± 0.01	0.296 ± 0.004
0.40	0.285 ± 0.002	0.30 ± 0.01	0.120 ± 0.003	0.30 ± 0.02

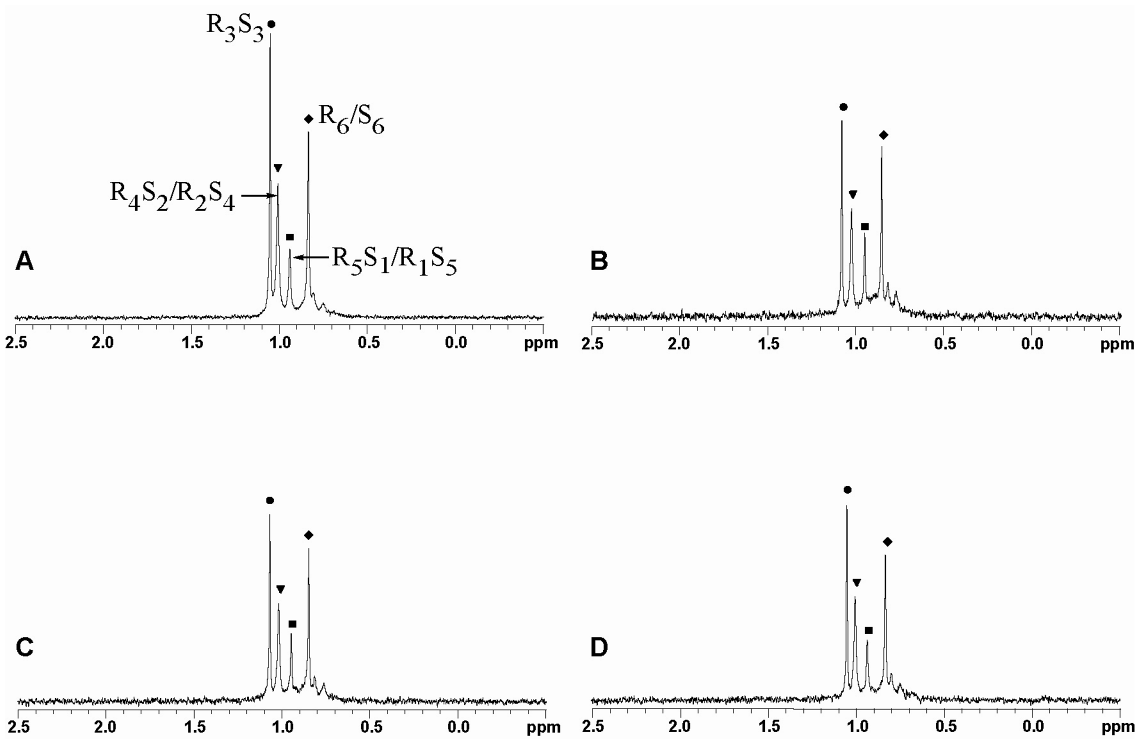

42. ^{6}Li NMR spectra recorded on a mixture of [^{6}Li](*R*)-**9** and [^{6}Li]*rac*-**9** (50% ee) in various THF/toluene mixtures at -50 °C: (A) 2.0 M; (B) 4.0 M; (C) 6.0 M; (D) 8.0 M. $\mathbf{R_3S_3}$ (•); $\mathbf{R_4S_2/R_2S_4}$ (▾); $\mathbf{R_5S_1/R_1S_5}$ (▪); $\mathbf{R_6/S_6}$ (◆). $\mathbf{R_nS_{N-n}/R_{N-n}S_n}$ and $\mathbf{R_N/S_N}$ refer to pairs of spectroscopically indistinguishable enantiomers.

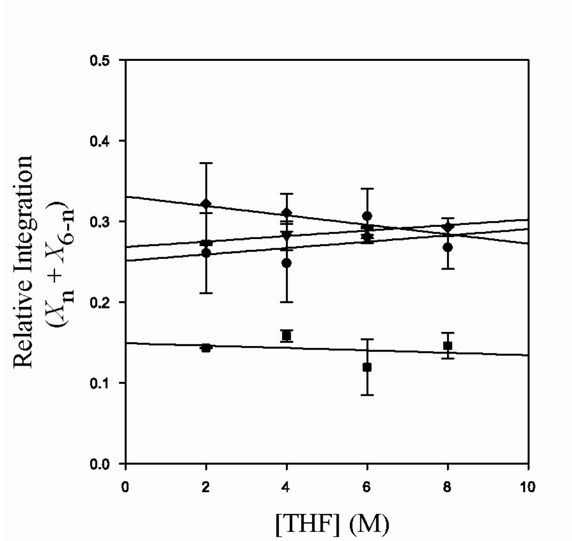

43. Plot of the mole fraction of the aggregate ($X_n + X_{6\text{-}n}$) versus [THF] for the spectra in Figure 42. For the case where n = 3, only X_3 is plotted. **R$_3$S$_3$** (●); **R$_4$S$_2$/R$_2$S$_4$** (▾); **R$_5$S$_1$/R$_1$S$_5$** (■); **R$_6$/S$_6$** (◆). **R$_n$S$_{N\text{-}n}$/R$_{N\text{-}n}$S$_n$** and **R$_N$/S$_N$** refer to pairs of spectroscopically indistinguishable enantiomers.

44. Table of data for the plot in Figure 43. ([^{6}Li](*R*)-**9** and [^{6}Li]*rac*-**9** (50% ee) in various THF concentrations (toluene co-solvent) at -50 °C.)

[THF] (M)	**R$_3$S$_3$**	**R$_4$S$_2$/R$_2$S$_4$**	**R$_5$S$_1$/R$_1$S$_5$**	**R$_6$/S$_6$**
2.0	0.26 ± 0.05	0.274 ± 0.001	0.143 ± 0.001	0.32 ± 0.05
4.0	0.25 ± 0.05	0.28 ± 0.02	0.16 ± 0.01	0.31 ± 0.02
6.0	0.31 ± 0.03	0.293 ± 0.001	0.12 ± 0.03	0.281 ± 0.002
8.0	0.27 ± 0.03	0.293 ± 0.001	0.15 ± 0.02	0.29 ± 0.01

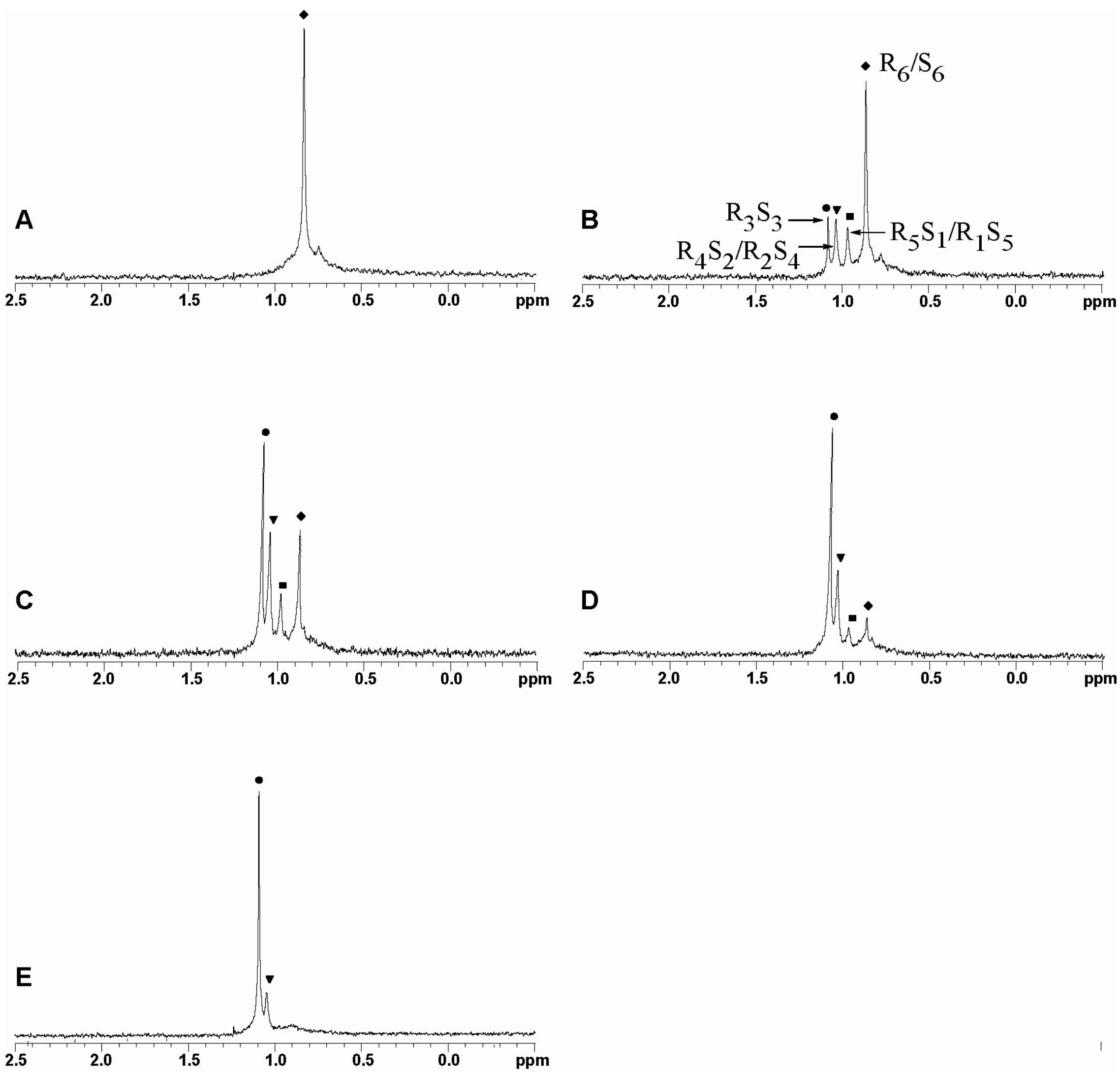

45. ^{6}Li NMR spectra recorded on mixtures of [^{6}Li](*S*)-**9** and [^{6}Li]*rac*-**9** ([enolate]$_{total}$ = 0.10 M) at -50 °C in 9.0 M THF/toluene: (A) X_R = 0.0 ; (B) X_R = 0.15; (C) X_R = 0.25; (D) X_R = 0.35; (E) X_R = 0.45. $\mathbf{R_3S_3}$ (●); $\mathbf{R_4S_2/R_2S_4}$ (▾); $\mathbf{R_5S_1/R_1S_5}$ (■); $\mathbf{R_6/S_6}$ (◆). $\mathbf{R_nS_{N-n}/R_{N-n}S_n}$ and $\mathbf{R_N/S_N}$ refer to pairs of spectroscopically indistinguishable enantiomers.

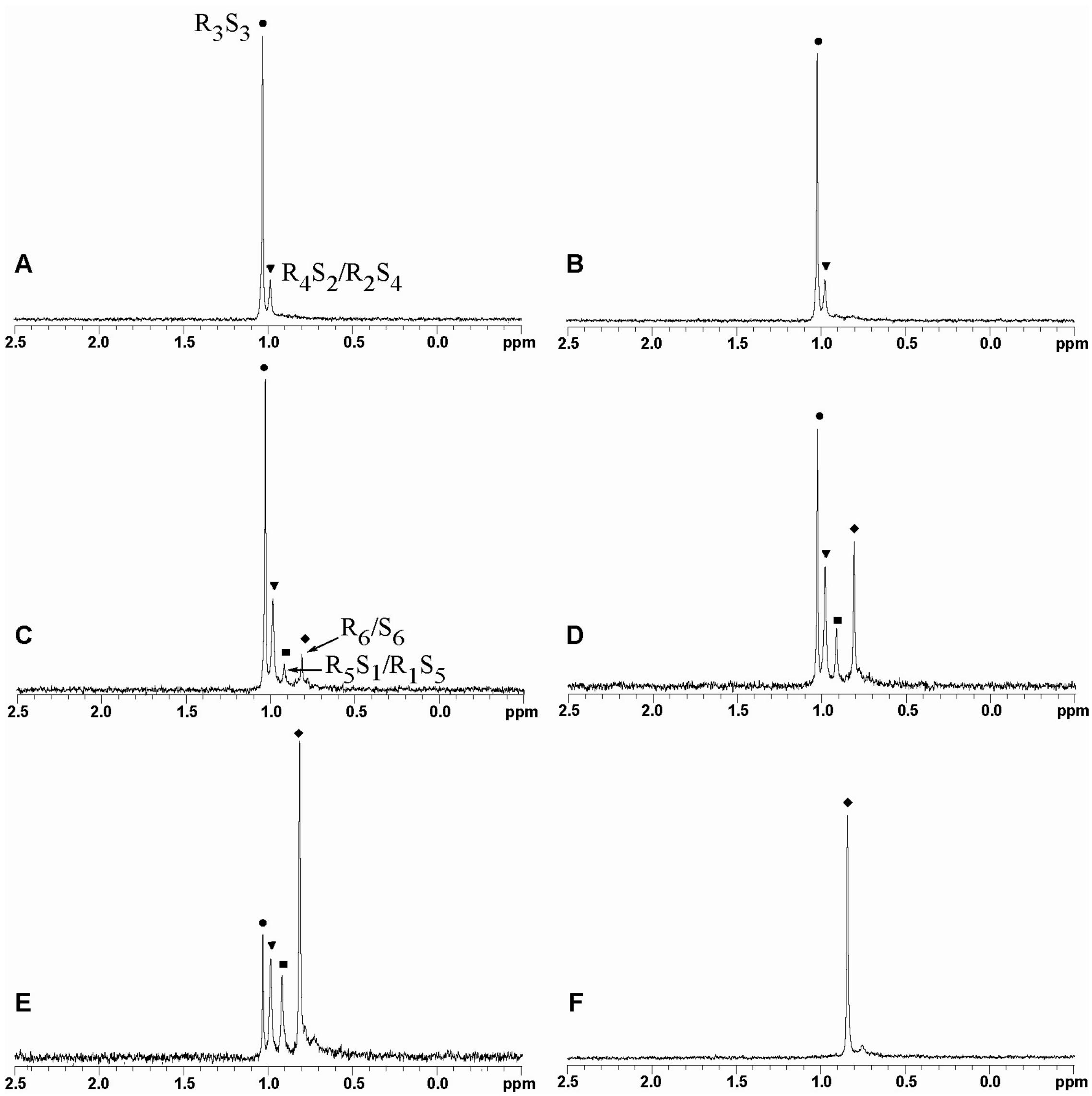

46. ^{6}Li NMR spectra recorded on mixtures of [^{6}Li](*R*)-**9** and [^{6}Li]*rac*-**9** ([enolate]$_{total}$ = 0.10 M) at -50 °C in 9.0 M THF/toluene: (A) X_R = 0.50 ; (B) X_R = 0.55; (C) X_R = 0.65; (D) X_R = 0.75; (E) X_R = 0.85; (F) X_R = 1.0. **R_3S_3** (●); **R_4S_2/R_2S_4** (▼); **R_5S_1/R_1S_5** (■); **R_6/S_6** (◆). **R_nS_{N-n}/$R_{N-n}S_n$** and **R_N/S_N** refer to pairs of spectroscopically indistinguishable enantiomers.

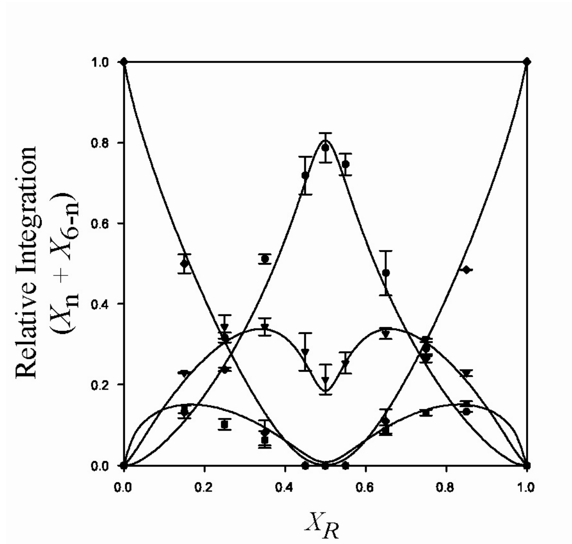

47. Plot of the mole fraction of the aggregate ($X_n + X_{6-n}$) versus the mole fraction of R (X_R) for the spectra in Figures 45 and 46. For the case where n = 3, only X_3 is plotted. $\mathbf{R_3S_3}$ (•); $\mathbf{R_4S_2/R_2S_4}$ (▾); $\mathbf{R_5S_1/R_1S_5}$ (▪); $\mathbf{R_6/S_6}$ (♦). $\mathbf{R_nS_{N-n}/R_{N-n}S_n}$ and $\mathbf{R_N/S_N}$ refer to pairs of spectroscopically indistinguishable enantiomers. See "Mathematical Derivations" section (pp S49-68) for details of the fit.

48. Table of data for the plot in Figure 47. (0.10 M [enolate]$_{total}$ at -50 °C in 9.0 M THF/toluene.)

X_R	$\mathbf{R_3S_3}$	$\mathbf{R_4S_2/R_2S_4}$	$\mathbf{R_5S_1/R_1S_5}$	$\mathbf{R_6/S_6}$
0.00	0.00 ± 0.00	0.00 ± 0.00	0.00 ± 0.00	1.00 ± 0.00
0.15	0.13 ± 0.02	0.230 ± 0.001	0.14 ± 0.01	0.50 ± 0.02
0.25	0.32 ± 0.01	0.34 ± 0.03	0.10 ± 0.01	0.238 ± 0.003
0.35	0.51 ± 0.01	0.34 ± 0.02	0.06 ± 0.02	0.08 ± 0.03
0.40	0.72 ± 0.05	0.28 ± 0.05	0.00 ± 0.00	0.00 ± 0.00
0.50	0.79 ± 0.04	0.21 ± 0.04	0.00 ± 0.00	0.00 ± 0.00
0.55	0.75 ± 0.03	0.25 ± 0.03	0.00 ± 0.00	0.00 ± 0.00
0.65	0.48 ± 0.06	0.33 ± 0.01	0.09 ± 0.01	0.11 ± 0.03
0.75	0.29 ± 0.02	0.314 ± 0.001	0.13 ± 0.01	0.27 ± 0.01
0.85	0.133 ± 0.001	0.23 ± 0.01	0.15 ± 0.01	0.485 ± 0.001
1.00	0.00 ± 0.00	0.00 ± 0.00	0.00 ± 0.00	1.00 ± 0.00

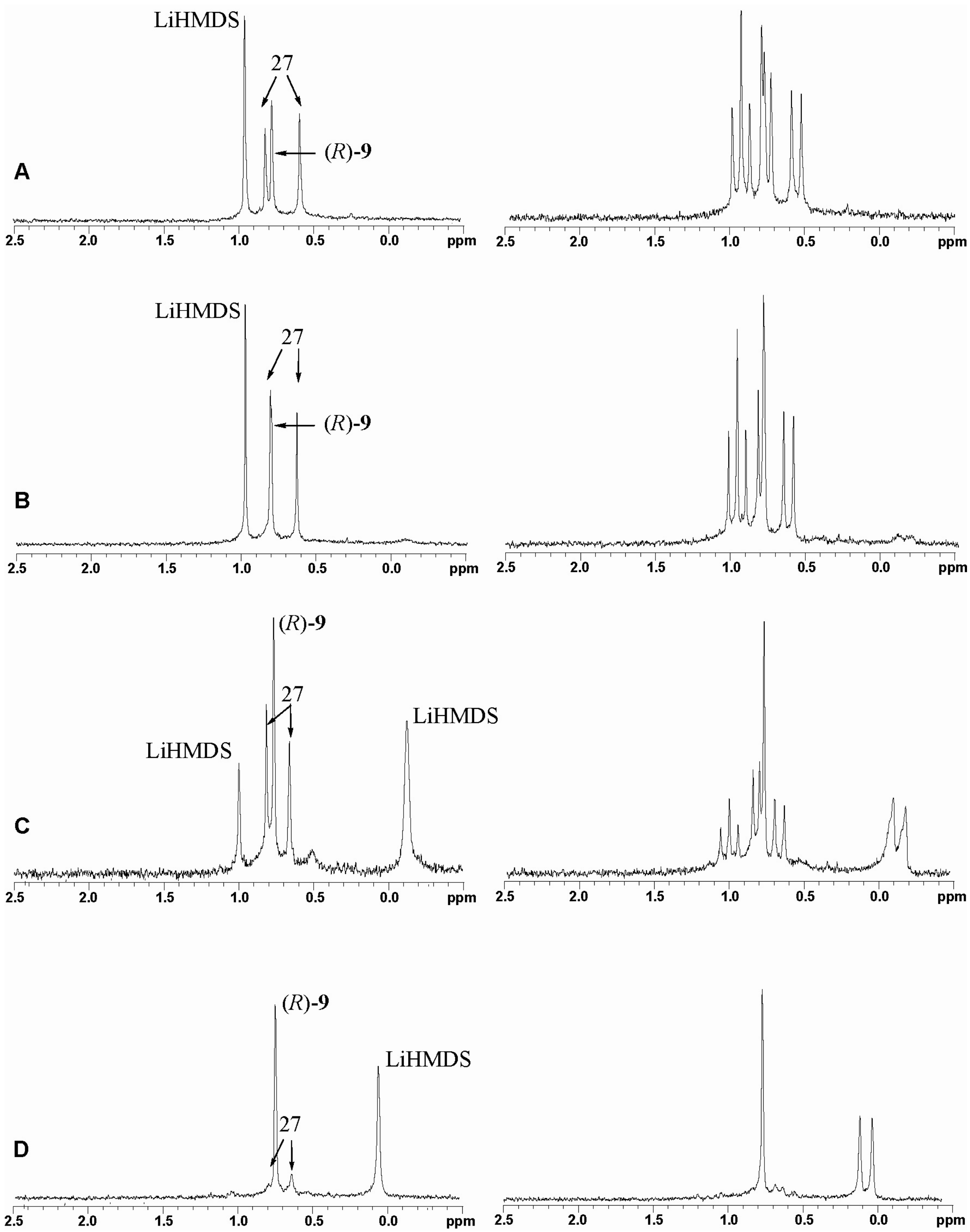

49. $^{6}Li\{^{15}N\}$ and ^{6}Li NMR spectra recorded on mixtures of [^{6}Li](*R*)-**9** (0.07 M) and [^{6}Li, ^{15}N]LiHMDS (0.07 M) at -90 °C in THF/toluene: (A) [THF] = 0.6 M; (B) [THF] = 3.1 M; (C) [THF] = 6.2 M; (D) [THF] = 12.3 M.

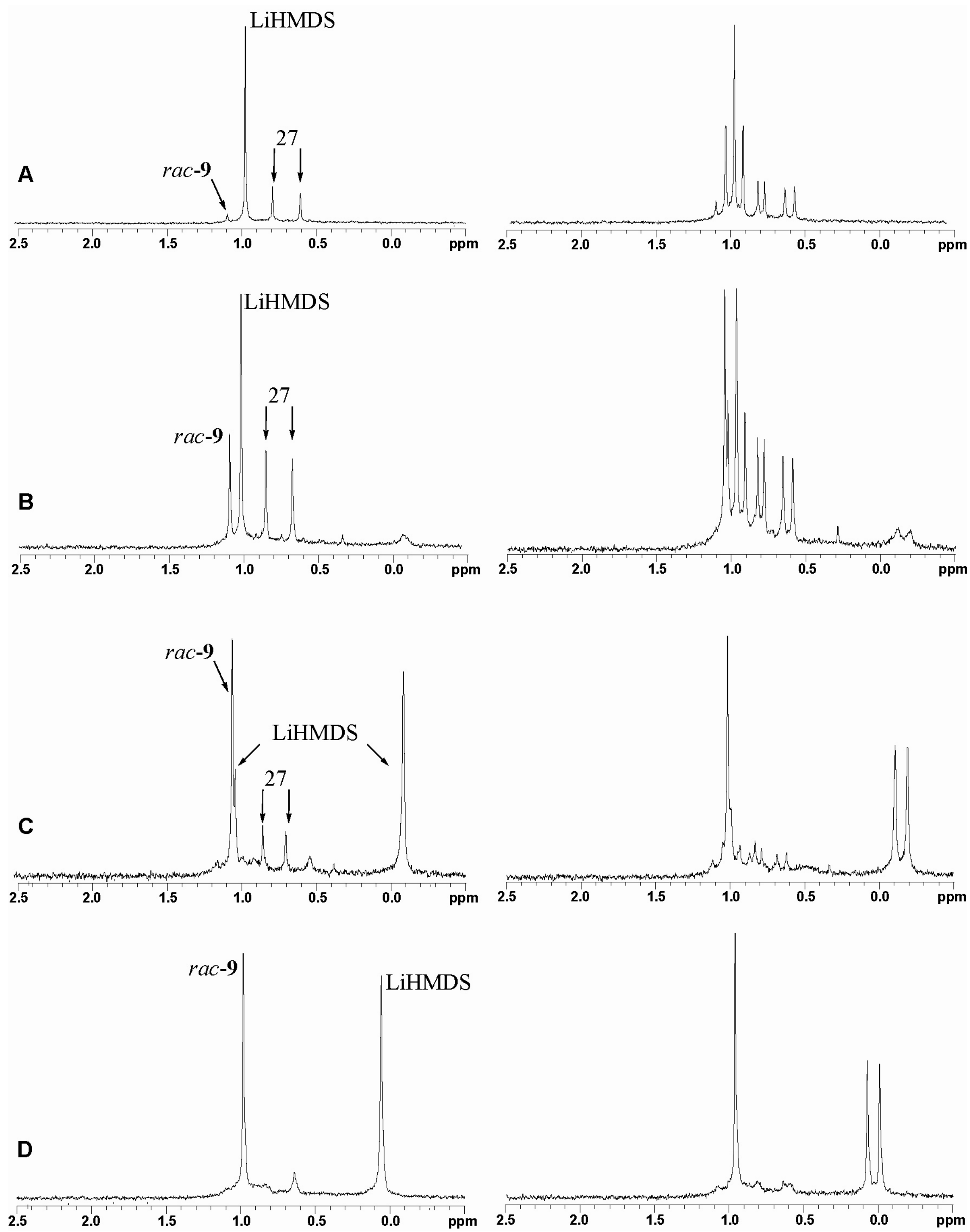

50. ^{6}Li{^{15}N} and ^{6}Li NMR spectra recorded on mixtures of [^{6}Li]*rac*-**9** (0.07 M) and [^{6}Li, ^{15}N]LiHMDS (0.07 M) at -90 ^{o}C in THF/toluene: (A) [THF] = 0.6 M; (B) [THF] = 3.1 M; (C) [THF] = 6.2 M; (D) [THF] = 12.3 M.

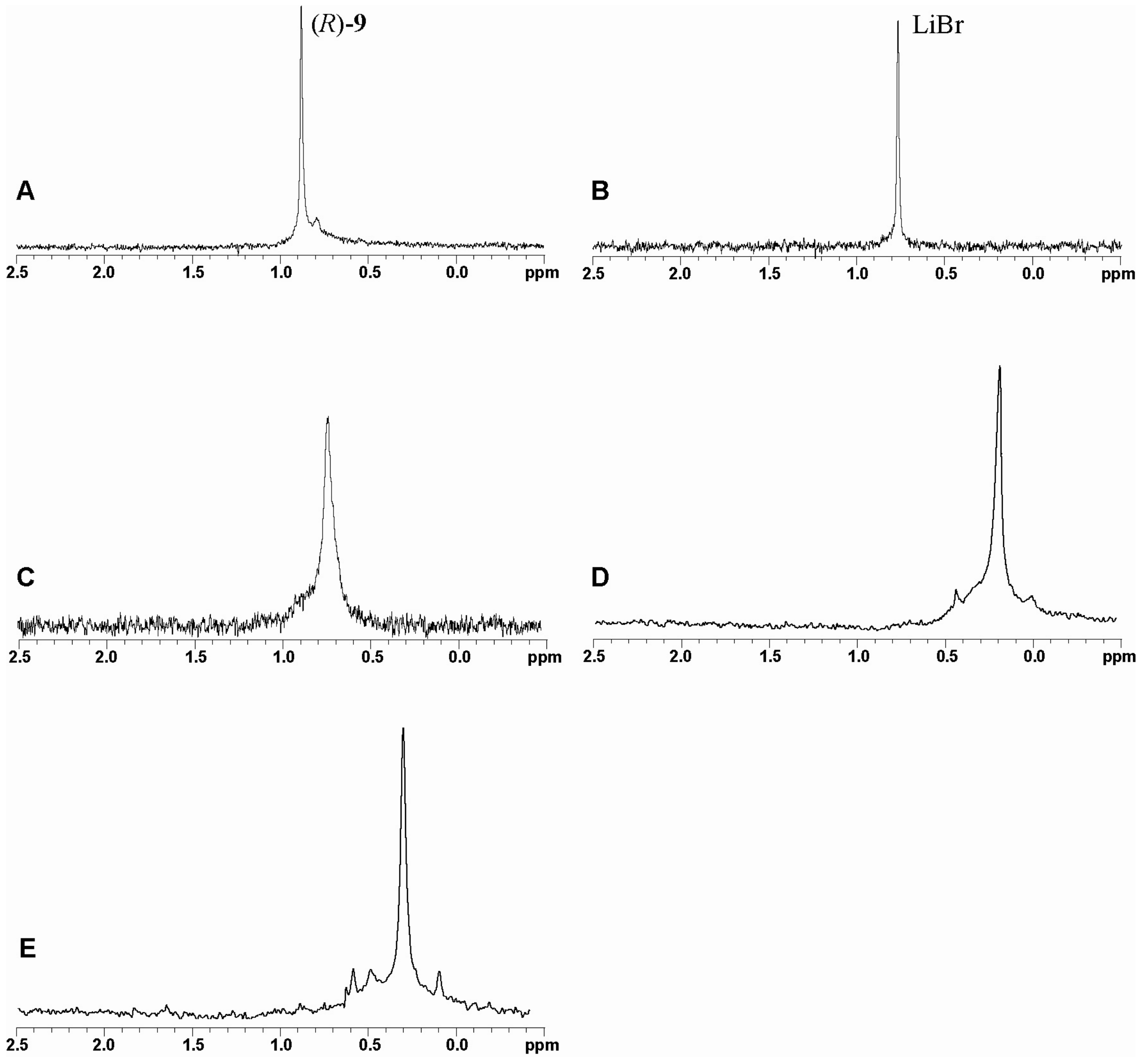

51. ^{6}Li NMR spectra recorded on mixtures of [^{6}Li](*R*)-**9** and [^{6}Li]LiBr in 9.0 M THF/toluene at various temperatures: (A) (*R*)-**9** (0.10 M), – 50 °C; (B) LiBr (0.10 M), – 50 °C; (C) (*R*)-**9**/LiBr (0.10 M/0.10 M), – 50 °C; (D) (*R*)-**9**/LiBr (0.10 M/0.10 M), – 70 °C; (E) (*R*)-**9**/LiBr (0.10 M/0.10 M), – 90 °C.

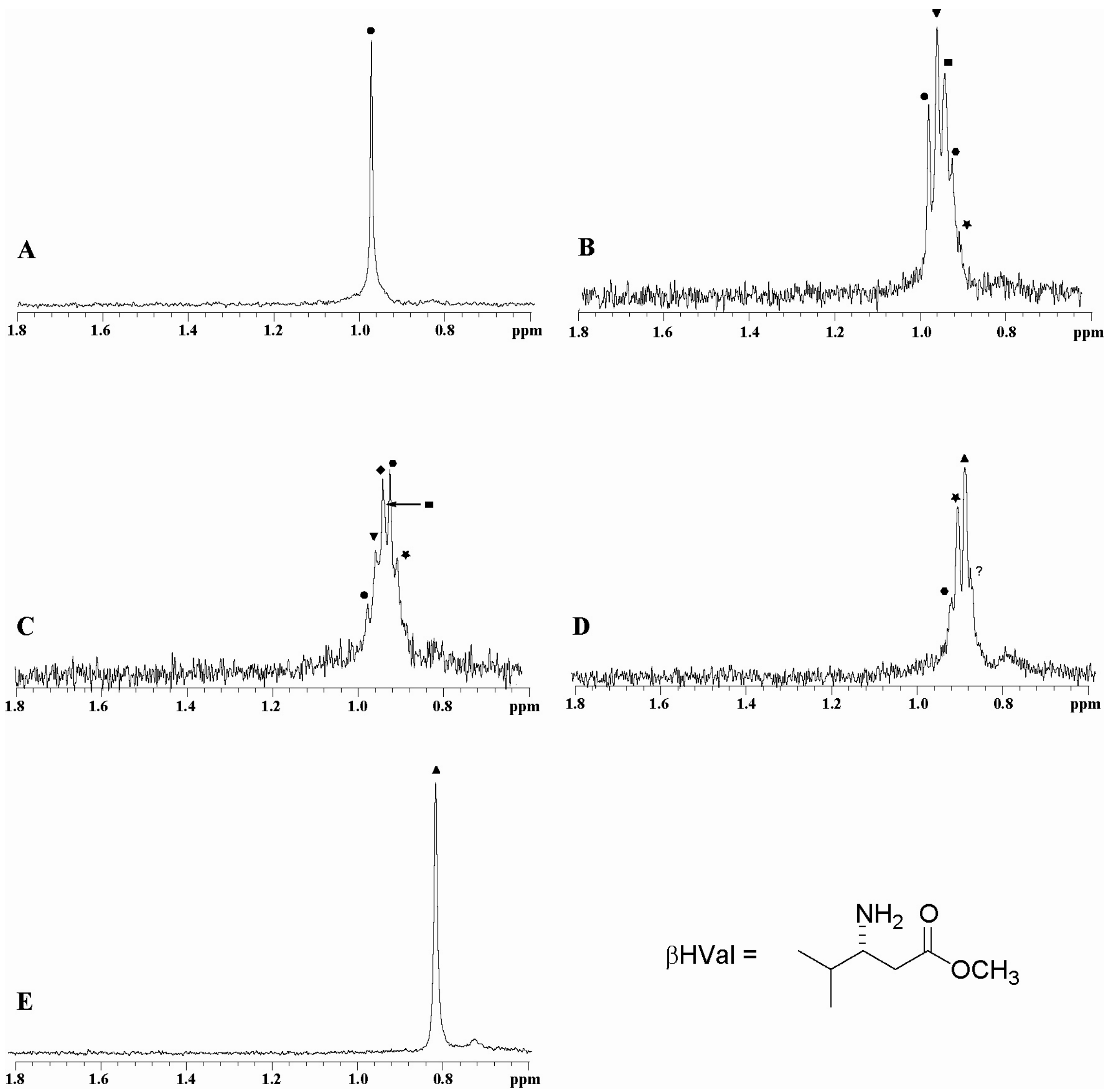

52. ^{6}Li NMR spectra recorded on mixtures of [^{6}Li](*R*)-**9** and [^{6}Li]βHVal in 9.8 M THF/cyclopentane at – 50 °C: (A) (*R*)-**9** (0.10 M); (B) (*R*)-**9**/βHVal (0.075 M/0.025 M); (C) (*R*)-**9**/βHVal (0.05 M/0.05 M); (D) (*R*)-**9**/βHVal (0.025 M/0.075 M); (E) βHVal (0.10 M).

MNDO Computations

MNDO computations were performed using WinMOPAC version 2.0 by Fujitsu© Limited.

53. Relative heats of formation (kcal/mol).

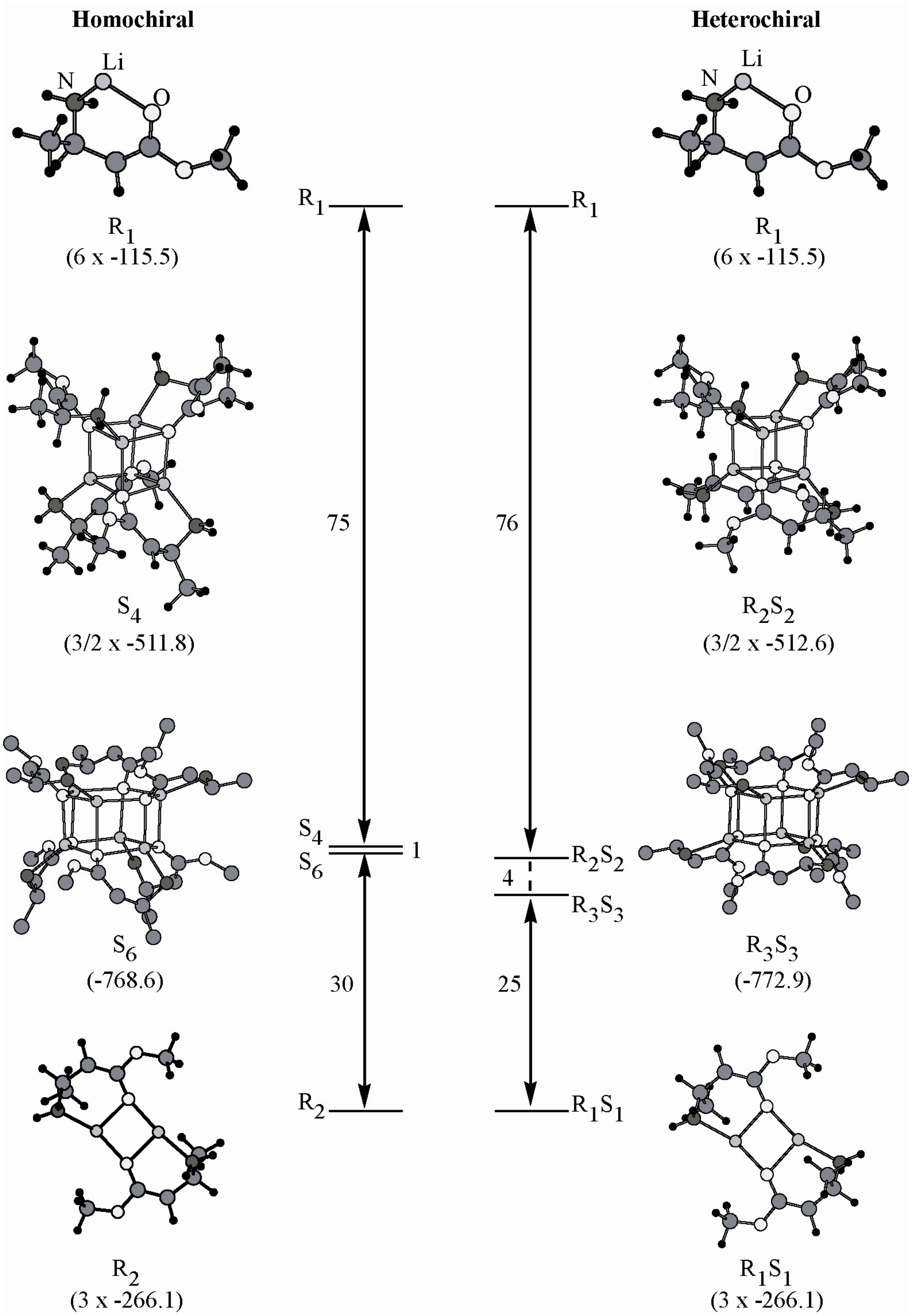

54. Effect of symmetry on heats of formation for hexamers (kcal/mol).

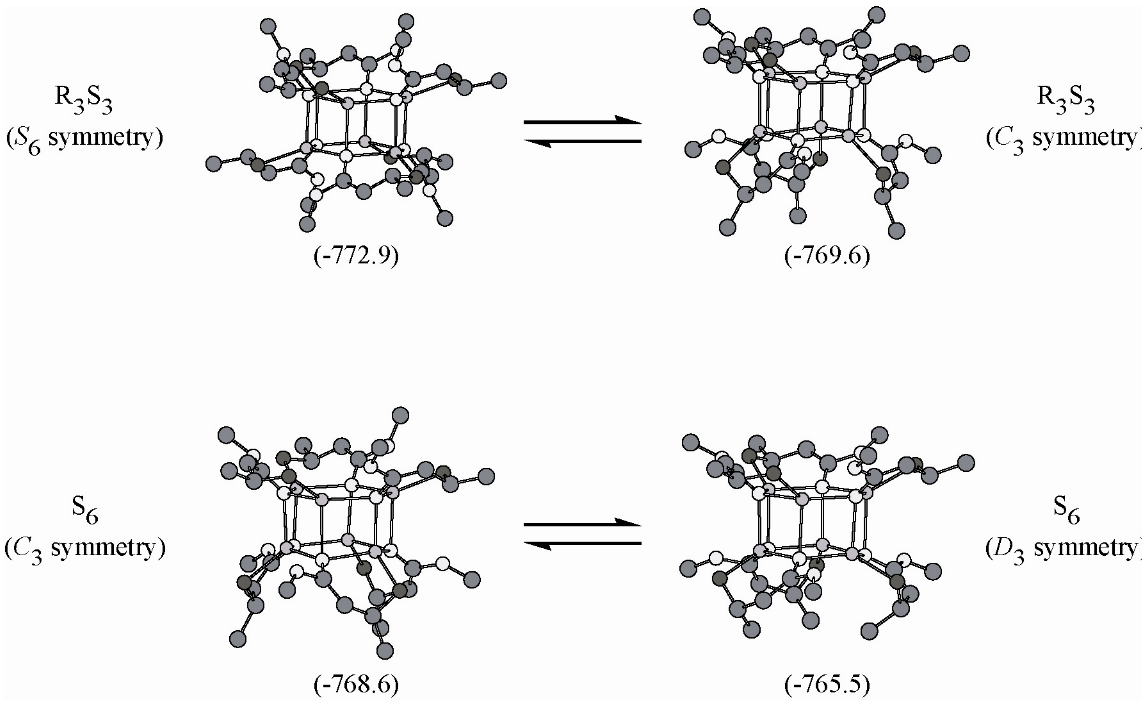

55. Thermoneutral opening of the R_3S_3 hexamer to the ladder (kcal/mol).

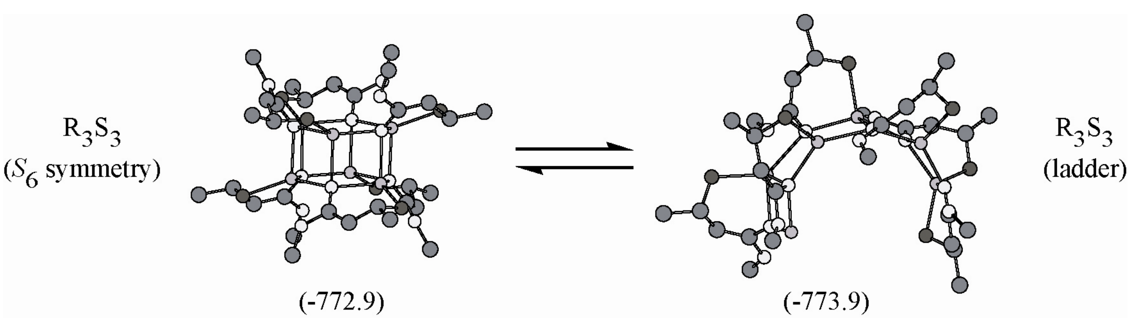

56. Transition structures for *anti* alkylation of the R_3S_3 ladder with CH_3Br (kcal/mol). Transition structures were verified by a single negative frequency at approximately -700 cm^{-1} which corresponding to the C-C-Br stretch.

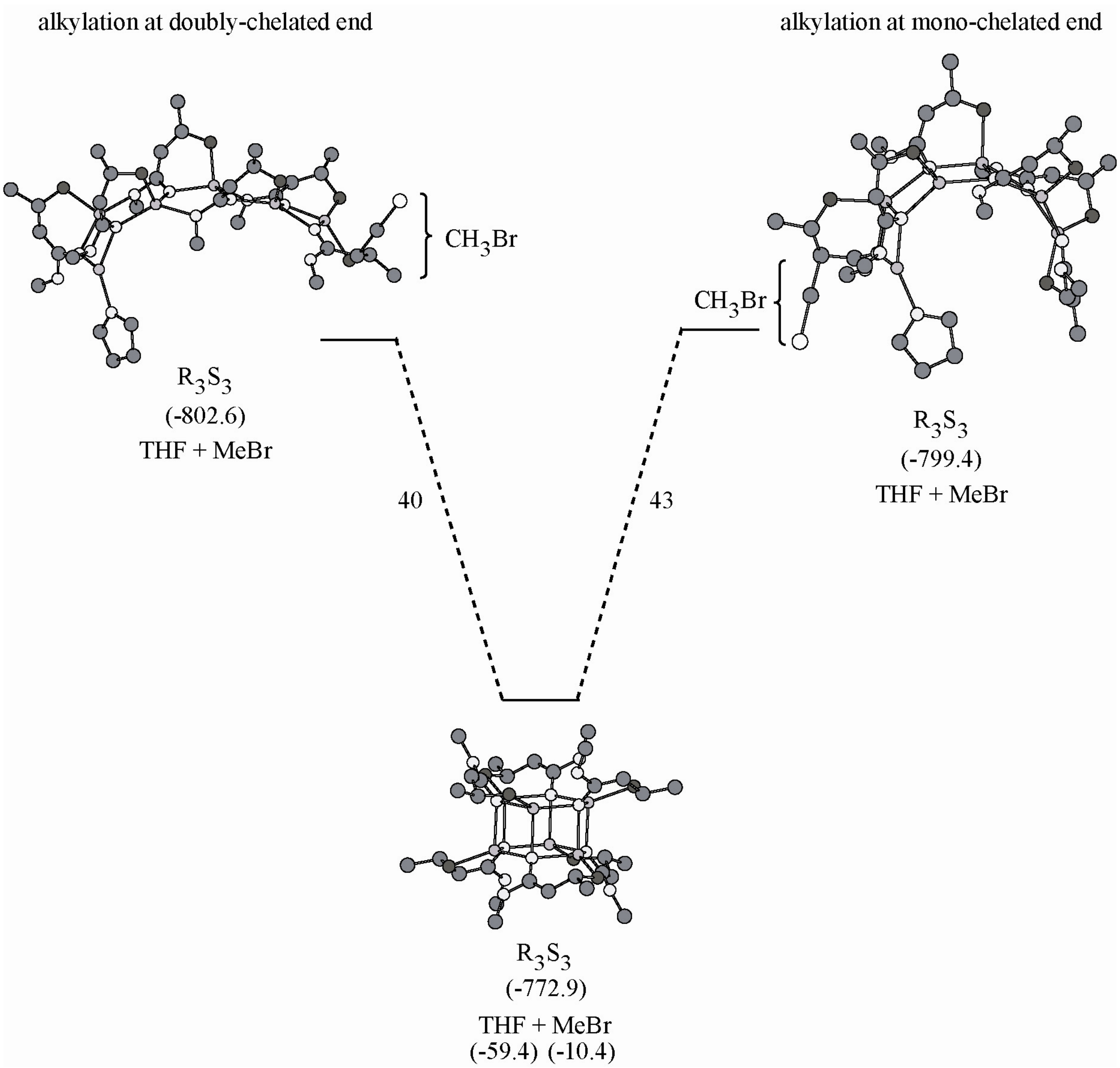

57. Transition structures for *anti* alkylation via a monomer with CH_3Br (kcal/mol).

Transition structures were verified by a single negative frequency at approximately -700 cm^{-1} which corresponding to the C-C-Br stretch.

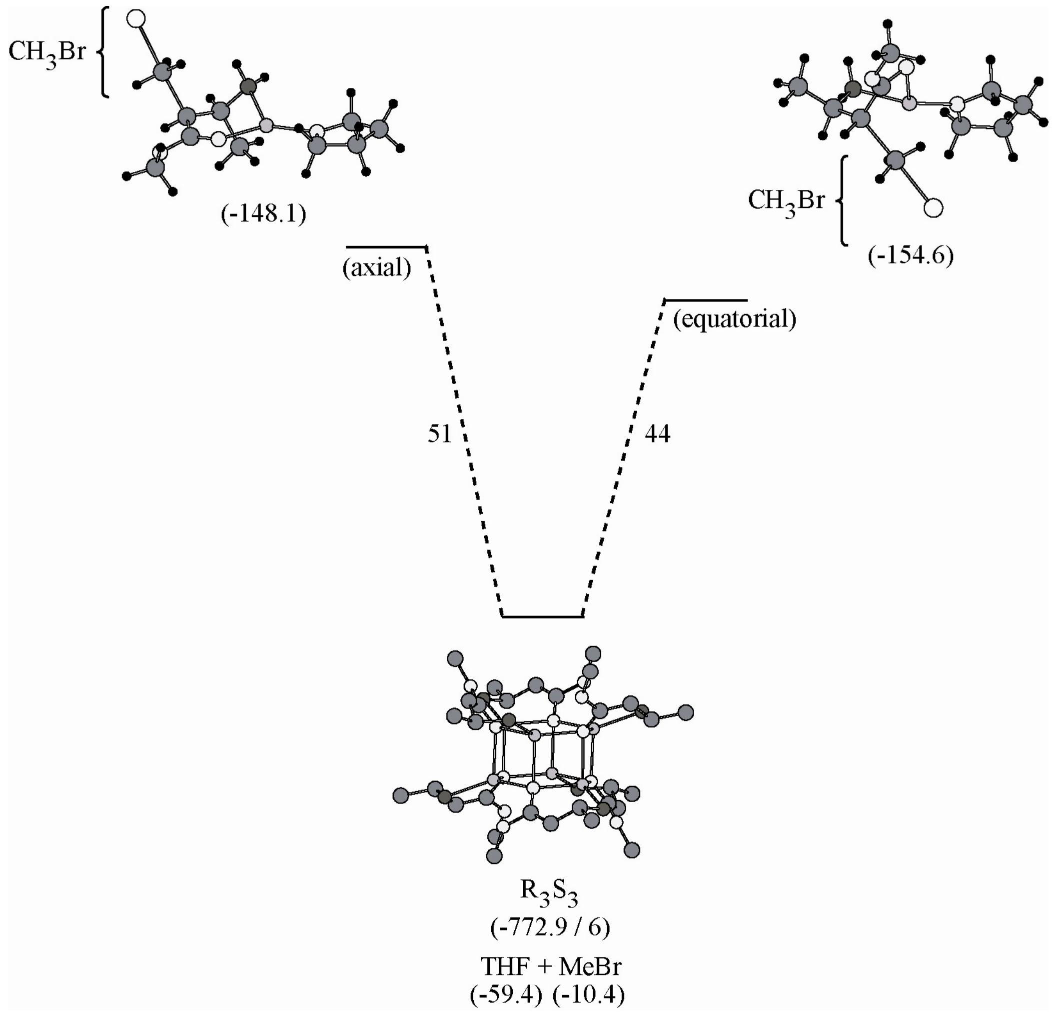

58. Transition structures for *anti* alkylation via a doubly-chelated dimer (R_1S_1) with CH_3Br (kcal/mol). Transition structures were verified by a single negative frequency at approximately -700 cm^{-1} which corresponding to the C-C-Br stretch.

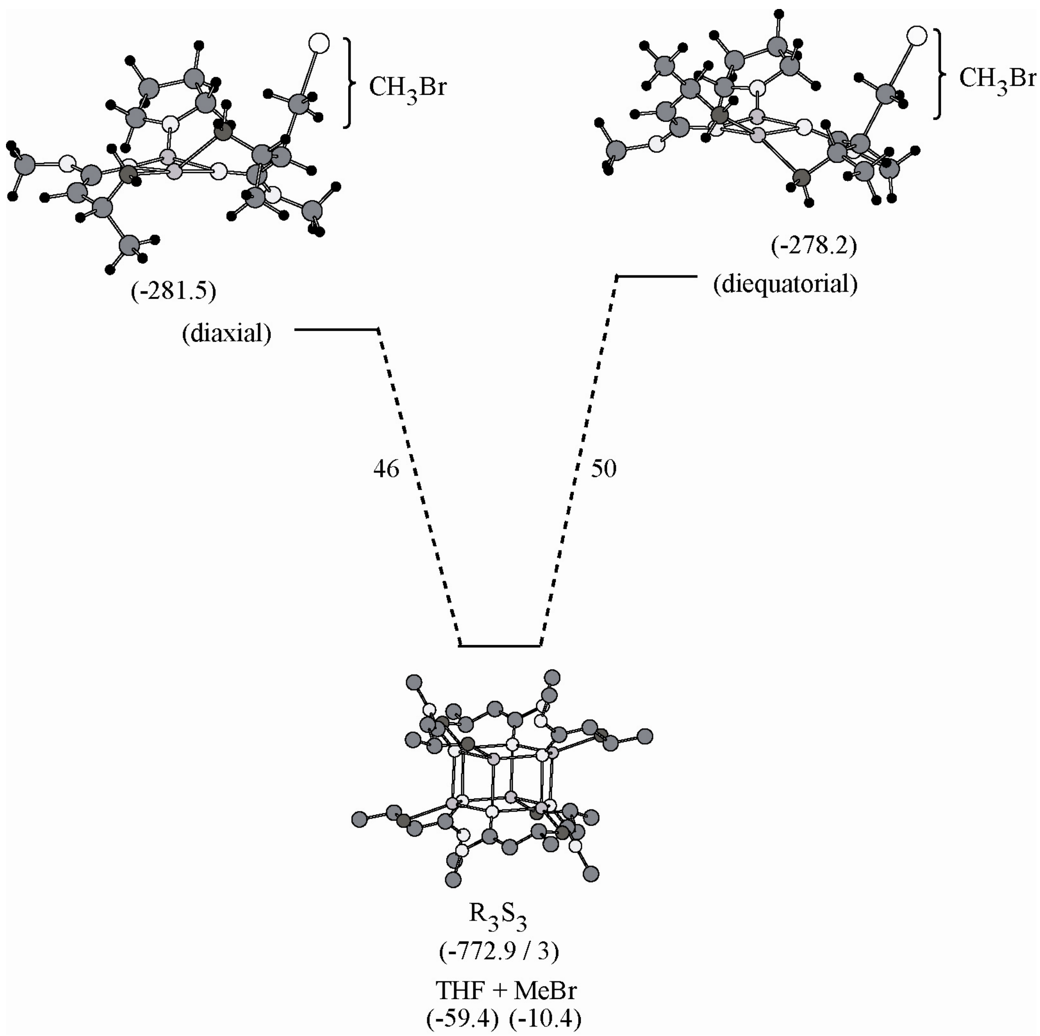

Mathematical Derivations

59. Introduction to the hexamer fitting protocol. We consider a situation where the two enantiomers, (*R*)-**9** and (*S*)-**9**, assemble in solution to form hexamers (N = 6). For an individual hexamer, each of the six positions in the assembly can be occupied by an (*R*)-**9** or an (*S*)-**9** (hereafter denoted as R and S, respectively). One way to describe a hexamer is by listing the occupant of each position – RSSRSR, RRRRRR, or RRSSRS for example. Rather than consider the concentration of each permutation, P, we can group them according to the number of R subunits in the hexamer, n_P. The concentration, $[R_nS_{N-n}]$, of states for which $n_P = n$ is given by the Boltzmann distribution. It will depend on

1. Multiplicity (M_n): The number of permutations of P for which $n_P = n$. By example, RSRSRS and SRRSSR are just two of 20 permutations with $n_P = 3$.

2. Free Energy (g_P): Each permutation may have a different energy of assembly/association. For example, RRRSSS may be a much less stable permutation than RSRSRS.

3. Chemical Potential (μ_R and μ_S): The total amount of R, $[R_{total}]$, and S, $[S_{total}]$, will set the chemical potentials and shift the likelihood of various states. If $[R_{total}] >> [S_{total}]$, for instance, then the $[R_1S_5]$ will be much less likely than $[R_5S_1]$.

In the experiment, the independent variable is the mole fraction of subunits of R, X_R, and the dependent variables are linear combinations of the mole fraction of $[R_nS_{N-n}]$, X_n. Thus, we wish to predict X_n as a function of X_R for a given model.

In Section 60 we use the Boltzmann distribution to give the value of $[R_nS_{N-n}]$ in terms of free energies, multiplicity and chemical potential. In Section 61 we give an explicit form for the multiplicity. The relationship between chemical potentials and $[R_{total}]$, $[S_{total}]$ (or X_R and X_S) is derived in Section 62.

Section 63 considers the case where the free energies of assembly for all the permutations are equal (statistical case) for which a simple analytic result is possible. As there are no model parameters in the statistical case, the data either fits the model or the statistical assumption is invalid.

The general case does not have a simple analytic solution. A parametric approach is described in Section 64. This numeric method allows one to compare the experimental and predicted populations, X_n, for a given set of free energies. We obtain the residual error after an iterative optimization of the free energies to fit the data, thus giving a measure of the model's validity. Section 65 describes the implementation of this approach. Section 66 relates free energies to equilibrium constants within the system. Section 67 shows a fit of the experimental data to a heptamer model. Sections 68 and 69 give the equations and sample plots for a model with tetramers and a dimer-tetramer mixture, respectively.

60. Boltzmann distribution. Consider a given permutation, P, with n_p subunits of type R and N-n_p subunits of type S. The Boltzmann distribution gives its equilibrium concentration as

$$[P] = C \times \exp\left(\frac{-g_p + n_P \mu_R + (N - n_P)\mu_S}{kT}\right)$$

where C is a constant, g_P is the free energy of assembly of P, μ_R is the chemical potential of R and μ_S is the chemical potential of S (Widom, B. *Statistical Mechanics: A Concise Introduction for Chemists*; Cambridge University Press: New York, 2002). Within the experiment, all states for which $n_P = n$ are indistinguishable. The concentration of permutations for which $n_p = n$ is given by

$$[R_n S_{N-n}] = \sum_{P;n_P=n} [P] = C \times \exp\left(\frac{n\mu_R + (N-n)\mu_S}{kT}\right) \times \sum_{P;n_P=n} \exp\left(\frac{-g_P}{kT}\right)$$
$$= C \times \exp\left(\frac{n\mu_R + (N-n)\mu_S}{kT}\right) \times M_n \times \left\langle \exp\left(\frac{-g_P}{kT}\right)\right\rangle_{P;n_p=n}$$

where M_n is the multiplicity (number of permutations P where $n_P = n$) and the average of free energy is taken over all states for which $n_P = n$. It is helpful to define some "effective" variables

$$r = \exp\left(\frac{\mu_R}{kT}\right) \qquad s = \exp\left(\frac{\mu_S}{kT}\right) \qquad \phi_n = \left\langle \exp\left(\frac{-g_P}{kT}\right)\right\rangle_{P;n_P=n}$$

Substituting these into the above expression gives

$$[R_n S_{N-n}] = C \times M_n \times \phi_n \times r^n \times s^{N-n} \qquad (1)$$

Increasing the chemical potential of R increases the value of "*r*" and favors the $[R_6S_0]$, $[R_5S_1]$, etc. states. Increasing the chemical potential of S increases the value of "*s*" which then favors $[R_0S_6]$, $[R_1S_5]$, etc.

φ_n describes the mean free energy of permutations in $[R_nS_{N-n}]$. Increasing φ_n favors $[R_nS_{N-n}]$ as would be expected if those states have a low free energy. Not all values of φ_n are independent.

The free energy of a permutation, P, and the free energy of one in which R and S have been exchanged are the same because the aggregates are enantiomers. This has the important consequence that

$$\phi_n = \phi_{N-n}$$

Furthermore, free energies can only be measured relative to the free energy of a reference state. For example, if free energies are measured relative to that of $[R_6S_0]$ then $\varphi_0 = \varphi_6 = 1$. When N is even, N/2 of the values of φ_n are independent. For example, when N = 6, φ_1 ,φ_2, and φ_3 are independent of each other.

61. Multiplicity. The value of M_n can be directly obtained by an exhaustive grouping of all hexamer permutations.

Species	n	M_n - Number of permutations	Permutations
R_0S_6	0	1	SSSSSS
R_1S_5	1	6	RSSSSS, SRSSSS, SSRSSS, SSSRSS, SSSSRS, SSSSSR
R_2S_4	2	15	RRSSSS, RSRSSS, RSSRSS, RSSSRS, RSSSSR, SRRSSS, SRSRSS, SRSSRS, SRSSSR, SSRRSS, SSRSRS, SSRSSR, SSSRRS, SSSRSR, SSSSRR
R_3S_3	3	20	RRRSSS, RRSRSS, RRSSRS, RRSSSR, RSRRSS, RSRSRS, RSRSSR, RSSRRS, RSSRSR, RSSSRR, + 10 other states with R and S switched
R_4S_2	4	15	SSRRRR, SRSRRR, SRRSRR, SRRRSR, SRRRRS, RSSRRR, RSRSRR, RSRRSR, RSRRRS, RRSSRR, RRSRSR, RRSRRS, RRRSSR, RRRSRS, RRRRSS
R_5S_1	5	6	SRRRRR, RSRRRR, RRSRRR, RRRSRR, RRRRSR, RRRRRS
R_6S_0	6	1	RRRRRR

Alternatively, one can use Pascal's triangle or the binomial theorem to achieve the general result

$$\text{Multiplicity} = \mathrm{M}_n = \frac{N!}{(N-n)!\times n!}.$$

62. Chemical potential. The experimental variables are the mole fractions of $[R_nS_{N-n}]$, X_n, and the mole fraction of R, X_R. Their relationships to C, *r* and *s* are described below.

Using eq 1 to compute $[R_nS_{N-n}]$, the mole fraction X_n is given by

$$X_n = \frac{[R_nS_{N-n}]}{\sum_{j=0}^{N}[R_jS_{N-j}]} = \frac{C\times M_n \times \phi_n \times r^n \times s^{N-n}}{\sum_{j=0}^{N} C\times M_j \times \phi_j \times r^j \times s^{N-j}} = \frac{M_n \times \phi_n \times \left(\frac{r}{s}\right)^n}{\sum_{j=0}^{N} M_j \times \phi_j \times \left(\frac{r}{s}\right)^j} \qquad (2)$$

$$= \frac{M_n \times \phi_n \times \exp\left(\frac{n\times(\mu_R - \mu_S)}{kT}\right)}{\sum_{j=0}^{N} M_j \times \phi_j \times \exp\left(\frac{j\times(\mu_R - \mu_S)}{kT}\right)}$$

which is independent of the value of C.

Permutations with $[R_nS_{N-n}]$ contain n subunits of R and N-n subunits of S. Thus, the mole fraction of R, X_R, is given by

$$X_R = \frac{[R]_{total}}{[R]_{total} + [S]_{total}} = \frac{\sum_{n=0}^{N} n\times[R_nS_{N-n}]}{\sum_{n=0}^{N} N\times[R_nS_{N-n}]}$$

$$= \frac{\sum_{n=0}^{N} n\times M_n \times \phi_n \times r^n \times s^{N-n}}{\sum_{n=0}^{N} N\times M_n \times \phi_n \times r^n \times s^{N-n}} = \frac{\sum_{n=0}^{N} n\times M_n \times \phi_n \times \left(\frac{r}{s}\right)^n}{\sum_{n=0}^{N} N\times M_n \times \phi_n \times \left(\frac{r}{s}\right)^n} \qquad (3)$$

All mole fractions depend only on the ratio *r/s* and φ_n, and X_R is a strictly monotonic function of *r/s*. Thus, if the mole fraction, X_R, and φ_n are known, eq 3 uniquely determines *r/s*. Knowing *r/s*, the value of any mole fraction, X_n, can be computed using eq 2.

In the special "statistical" case there is a simple analytic form for *r/s*. This case is examined in Section 63. For the general case, *r/s* is most easily determined numerically. A parametric approach is described in Sections 64 and 65.

63. The statistical case. Eq 3 can be considerably simplified if every permutation (RRSRRS, SRRRRR, etc.) has the same free energy. In this case, ϕ_n is independent of n so eq 3 simplifies to

$$X_R = \frac{\sum_{n=0}^{N} nM_n \phi_n r^n s^{N-n}}{\sum_{n=0}^{N} NM_n \phi_n r^n s^{N-n}} = \frac{\sum_{n=0}^{N} nM_n r^n s^{N-n}}{\sum_{n=0}^{N} NM_n r^n s^{N-n}}$$
$$= \frac{\sum_{n=0}^{N} n \times \frac{N!}{n!(N-n)!} \times r^n \times s^{N-n}}{\sum_{n=0}^{N} N \times \frac{N!}{n!(N-n)!} \times r^n \times s^{N-n}}$$

Using the binomial expansion

$$\sum_{j=0}^{N} \frac{N!}{j!(N-j)!} a^j b^{N-j} = (a+b)^N$$

gives

$$X_R = \frac{N \times r \times (r+s)^{N-1}}{N \times (r+s)^N} = \frac{r}{r+s} \quad \leftrightarrow \quad \frac{r}{s} = \frac{X_R}{1-X_R} \tag{4}$$

which is an explicit expression for *r/s* as a function of X_R. Substituting eq 4 into eq 2 determines the concentration of any species in solution in terms of X_R. The mole fraction of $[R_nS_{N-n}]$, X_n, is equal to

$$X_n = \frac{M_n \times \phi_n \times r^n \times s^{N-n}}{\sum_{j=0}^{N} M_j \times \phi_j \times r^j s^{N-j}} = \frac{\frac{N!}{n!(N-n)!} \times r^n \times s^{N-n}}{\sum_{j=0}^{N} \frac{N!}{j!(N-j)!} \times r^j \times s^{N-j}} = \frac{N!}{n!(N-n)!} \times \frac{r^n \times s^{N-n}}{(r+s)^N} \tag{5}$$
$$= \frac{N!}{n!(N-n)!} \times X_R^n \times (1-X_R)^{N-n}$$

The experiment measures combinations of $X_n + X_{6\text{-}n}$. For the specific case of N = 6,

Mole fraction of $[R_0S_6] + [R_6S_0] = X_0 + X_6$

Mole fraction of $[R_1S_5] + [R_5S_1] = X_1 + X_5$

Mole fraction of $[R_2S_4] + [R_4S_2] = X_2 + X_4$

Mole fraction of $[R_3S_3] = X_3$

Using eq 5 these are equal to,

Mole fraction of $[R_0S_6] + [R_6S_0] = X_R^6 + (1 - X_R)^6$

Mole fraction of $[R_1S_5] + [R_5S_1] = 6X_R^5(1 - X_R) + 6X_R(1 - X_R)^5$

Mole fraction of $[R_2S_4] + [R_4S_2] = 15X_R^4(1 - X_R)^2 + 15X_R^2(1 - X_R)^4$

Mole fraction of $[R_3S_3] = 20X_R^3(1 - X_R)^3$

The above formulae are used to plot all four populations as a function of X_R. Because there are no free parameters, the experimental data either matches this plot, or the assumption that φ_n does not depend on n is wrong.

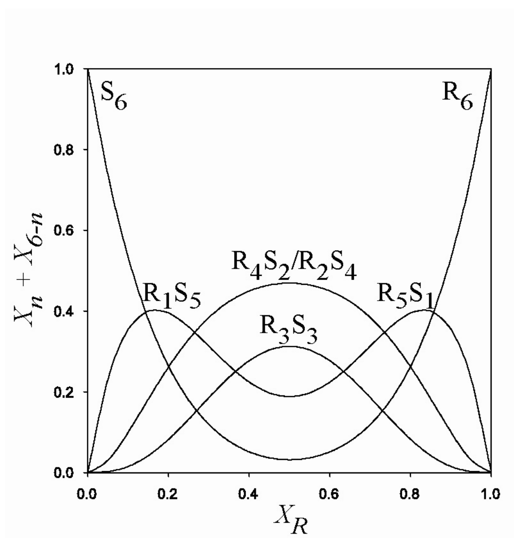

64. The parametric method. In general, each permutation can differ in stability, so φ_n depends on n. In this case, there is not a simple analytic expression for X_n as a function of X_R and φ_n. However, eqs 2 and 3 permit one to evaluate X_R and X_n as functions of r/s. For example, when N = 6, the total mole fraction of R is

$$X_R = \frac{\sum_{n=0}^{N} nM_n\phi_n r^n s^{N-n}}{\sum_{n=0}^{N} NM_n\phi_n r^n s^{N-n}} = \frac{\phi_1 r^1 s^5 + 5\phi_2 r^2 s^4 + 10\phi_3 r^3 s^3 + 10\phi_4 r^4 s^2 + 5\phi_5 r^5 s^1 + \phi_6 r^6}{\phi_0 s^6 + 6\phi_1 r^1 s^5 + 15\phi_2 r^2 s^4 + 20\phi_3 r^3 s^3 + 15\phi_4 r^4 s^2 + 6\phi_5 r^5 s^1 + \phi_6 r^6} \quad (6)$$

and the experimentally measured mole fractions, X_n, are

$$X_0 + X_6 = \frac{\phi_0 s^6 + \phi_6 r^6}{\phi_0 s^6 + 6\phi_1 r^1 s^5 + 15\phi_2 r^2 s^4 + 20\phi_3 r^3 s^3 + 15\phi_4 r^4 s^2 + 6\phi_5 r^5 s^1 + \phi_6 r^6} \quad (7)$$

$$X_1 + X_5 = \frac{6\left(\phi_1 r^1 s^5 + \phi_5 r^5 s^1\right)}{\phi_0 s^6 + 6\phi_1 r^1 s^5 + 15\phi_2 r^2 s^4 + 20\phi_3 r^3 s^3 + 15\phi_4 r^4 s^2 + 6\phi_5 r^5 s^1 + \phi_6 r^6} \quad (8)$$

$$X_2 + X_4 = \frac{15\left(\phi_2 r^2 s^4 + \phi_4 r^4 s^2\right)}{\phi_0 s^6 + 6\phi_1 r^1 s^5 + 15\phi_2 r^2 s^4 + 20\phi_3 r^3 s^3 + 15\phi_4 r^4 s^2 + 6\phi_5 r^5 s^1 + \phi_6 r^6} \quad (9)$$

$$X_3 = \frac{20\phi_3 r^3 s^3}{\phi_0 s^6 + 6\phi_1 r^1 s^5 + 15\phi_2 r^2 s^4 + 20\phi_3 r^3 s^3 + 15\phi_4 r^4 s^2 + 6\phi_5 r^5 s^1 + \phi_6 r^6} \quad (10)$$

For a given value of X_R and φ_n, one may determine the required value of r/s via numeric inversion of eq 6 or by graphing X_R versus r. Using the obtained value r/s and eqs 7-10, one can then compute the populations. A graphical depiction of the parametric approach is described below for the case where $\varphi_0 = \varphi_6 = 1$, $\varphi_1 = \varphi_5 = 1.5$, $\varphi_2 = \varphi_4 = 5$, $\varphi_3 = 10$.

Since the above equations only depend on the ratio, r/s, for convenience we may define

$$s = 1 - r \quad \leftrightarrow \quad \frac{r}{s} = \frac{r}{1-r}$$

Using eq 6, we obtain the following plot for the example where $\varphi_0 = \varphi_6 = 1$, $\varphi_1 = \varphi_5 = 1.5$, $\varphi_2 = \varphi_4 = 5$, $\varphi_3 = 10$.

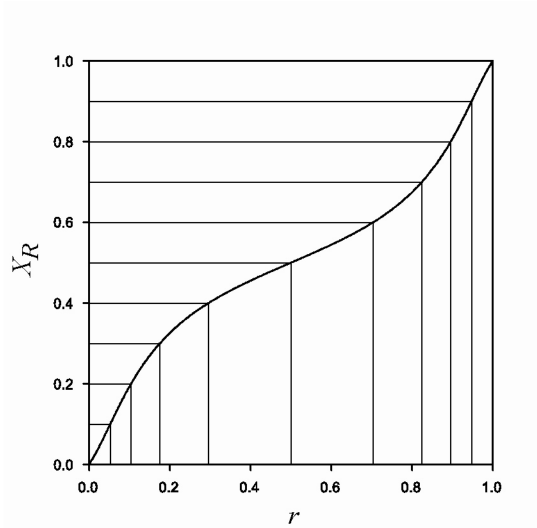

The drop lines depicted for each X_R allow one to determine the corresponding value of r. For this example we obtain the following values of r at each X_R.

X_R	r	r/s
0	0	0
0.1	0.0522	0.0551
0.2	0.104	0.116
0.3	0.175	0.213
0.4	0.296	0.421
0.5	0.50	1.0
0.6	0.704	2.377
0.7	0.825	4.706
0.8	0.896	8.643
0.9	0.948	18.14
1.0	1.0	infinity

Using these values of r/s, we compute $X_0 + X_6$, $X_1 + X_5$, $X_2 + X_4$, and X_3 using eqs 7-10. The results are plotted below.

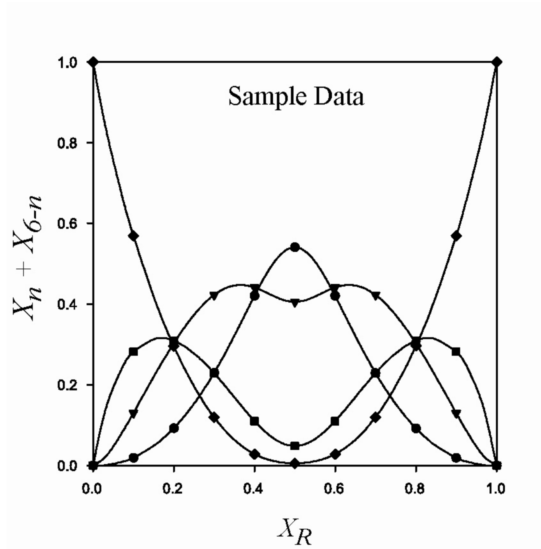

R_3S_3 (●); **R_4S_2/R_2S_4** (▼); **R_5S_1/R_1S_5** (■); **R_6/S_6** (◆).

Comparing the above plot with the plot obtained in the statistical case (Section 63), there are several notable changes. For instance, the **R_4S_2/R_2S_4** curve now exhibits two maxima. Also, at X_R = 0.5, the dominant species is now **R_3S_3**. These results match our expectations because φ_3 was set to be larger than all other φ_n's ($\varphi_0 = \varphi_6 = 1$, $\varphi_1 = \varphi_5 = 1.5$, $\varphi_2 = \varphi_4 = 5$, $\varphi_3 = 10$).

65. Fitting the experimental data with the parametric method. To compare the theory directly to experiment, one can refine an initial guess of φ_n until the predicted populations for the experimental values of X_R best fit the experimental populations. An adaptive step algorithm iteratively adjusts φ_n to minimize the root mean square error in the predicted populations. N/2 of the φ_n variables are independent, and for N = 6, φ_1, φ_2, and φ_3 are a convenient choice. A software package that supports nonlinear least-squares fitting of parametric equations is required. The root mean square deviation between the hexamer model and the data is 2.9%.

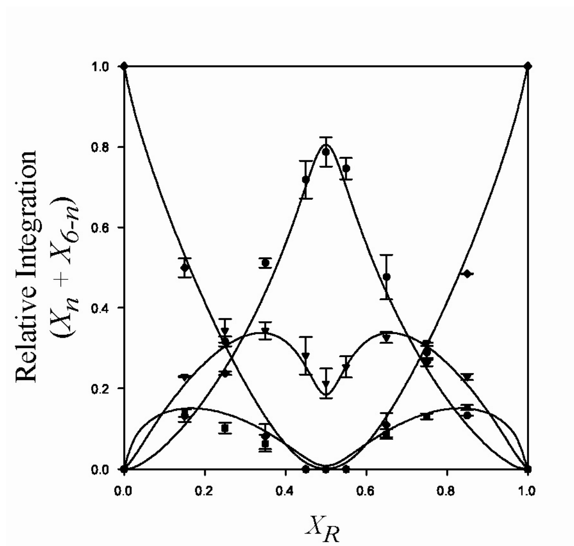

(•) R_3S_3; (▾) R_4S_2/R_2S_4; (▪) R_5S_1/R_1S_5; (♦) R_6/S_6.

Best fit values of φ

φ_0	φ_1	φ_2	φ_3	φ_4	φ_5	φ_6
1.0	0.79	7.3	47.7	7.3	0.79	1.0

Percent Errors in φ_n

n	0	1	2	3
φ_n/φ_o	0	3.7	6.5	9.4
φ_n/φ_1	3.7	0	3.7	6.5
φ_n/φ_2	6.5	3.7	0	2.8
φ_n/φ_3	9.4	6.5	2.8	0

66. Equilibrium constants. The "free energy coefficients" of R_nS_{N-n} (φ_n) are related to the equilibrium constants as follows

$$R_3S_3 \overset{K_1}{\rightleftharpoons} \tfrac{1}{2}\,R_6 \quad + \quad \tfrac{1}{2}\,S_6$$

$$R_3S_3 \overset{K_2}{\rightleftharpoons} \tfrac{1}{2}\,R_5S_1 + \tfrac{1}{2}\,R_1S_5$$

$$R_3S_3 \overset{K_3}{\rightleftharpoons} \tfrac{1}{2}\,R_4S_2 + \tfrac{1}{2}\,R_2S_4$$

We now express K_1, K_2 and K_3 in terms of φ_n using eq 1.

$$K_1 = \frac{[R_6]^{1/2} \times [S_6]^{1/2}}{[R_3S_3]}$$

Substituting the concentrations into eq 1

$$[S_6] = C \times M_0 \times \phi_0 \times s^6 \quad [R_6] = C \times M_6 \times \phi_6 \times r^6 \quad [R_3S_3] = C \times M_3 \times \phi_3 \times r^3 \times s^3$$

which then give,

$$K_1 = \frac{\left(CM_0\phi_0 s^6\right)^{1/2} \times \left(CM_6\phi_6 r^6\right)^{1/2}}{\left(CM_3\phi_3 r^3 s^3\right)} = \frac{\phi_0}{20\phi_3}$$

For the above reactions,

$$K_1 = \frac{\phi_0}{20\phi_3} \qquad K_2 = \frac{3\phi_1}{10\phi_3} \qquad K_3 = \frac{3\phi_2}{4\phi_3}$$

For the general case,

$$aR_{n_a}S_{N-n_a} + bR_{n_b}S_{N-n_b} \overset{K}{\rightleftharpoons} cR_{n_c}S_{N-n_c} + dR_{n_d}S_{N-n_d}$$

$$K = \frac{\left(M_{n_c}\phi_{n_c}\right)^c \times \left(M_{n_d}\phi_{n_d}\right)^d}{\left(M_{n_a}\phi_{n_a}\right)^a \times \left(M_{n_b}\phi_{n_b}\right)^b}$$

m	$K_{statistical}$	$\Delta G_{statistical}$ (kcal/mol)[a]	$K_{experimental}$	$\Delta G_{non\text{-}statistical}$ (kcal/mol)[b]
1	0.05	1.33	$1.0 \pm 0.1 \times 10^{-3}$	1.73 ± 0.04
2	0.30	0.53	$5.0 \pm 0.3 \times 10^{-3}$	1.82 ± 0.03
3	0.75	0.13	$115 \pm 3 \times 10^{-3}$	0.83 ± 0.01

[a] $\Delta G_{statistical} = - RT\ln K_{statistical}$

[b] $\Delta G_{non\text{-}statistical} = - RT\ln(K_{experimental}/K_{statistical})$

.

67. **Heptamer fit to data.** If the subunits assemble into heptamers, the concentration of $[R_nS_{7-n}]$ can be written using eq 1.

$$[R_nS_{7-n}] = C \times \frac{7!}{(7-n)! \times n!} \times \phi_n \times r^n \times s^{7-n}$$

Similarly, from eqs 2 and 3, the mole fraction of subunits of R, X_R, is given by

$$X_R = \frac{\sum_{n=0}^{N} n \times M_n \times \phi_n \times r^n \times s^{N-n}}{\sum_{n=0}^{N} N \times M_n \times \phi_n \times r^n \times s^{N-n}}$$
$$= \frac{\phi_1 r^1 s^6 + 6\phi_2 r^2 s^5 + 15\phi_3 r^3 s^4 + 20\phi_4 r^4 s^3 + 15\phi_5 r^5 s^2 + 6\phi_6 r^6 s^1 + \phi_7 r^7}{\phi_0 r^0 s^7 + 7\phi_1 r^1 s^6 + 21\phi_2 r^2 s^5 + 35\phi_3 r^3 s^4 + 35\phi_4 r^4 s^3 + 21\phi_5 r^5 s^2 + 7\phi_6 r^6 s^1 + \phi_7 r^7}$$

and the experimentally measured mole fractions, X_n, are

$$X_0 + X_7 = \frac{\phi_0 s^7 + \phi_7 r^7}{\phi_0 s^7 + 7\phi_1 r^1 s^6 + 21\phi_2 r^2 s^5 + 35\phi_3 r^3 s^4 + 35\phi_4 r^4 s^3 + 21\phi_5 r^5 s^2 + 7\phi_6 r^6 s^1 + \phi_7 r^7}$$

$$X_1 + X_6 = \frac{7\left(\phi_1 r^1 s^6 + \phi_6 r^6 s^1\right)}{\phi_0 s^7 + 7\phi_1 r^1 s^6 + 21\phi_2 r^2 s^5 + 35\phi_3 r^3 s^4 + 35\phi_4 r^4 s^3 + 21\phi_5 r^5 s^2 + 7\phi_6 r^6 s^1 + \phi_7 r^7}$$

$$X_2 + X_5 = \frac{21\left(\phi_2 r^2 s^5 + \phi_5 r^5 s^2\right)}{\phi_0 s^7 + 7\phi_1 r^1 s^6 + 21\phi_2 r^2 s^5 + 35\phi_3 r^3 s^4 + 35\phi_4 r^4 s^3 + 21\phi_5 r^5 s^2 + 7\phi_6 r^6 s^1 + \phi_7 r^7}$$

$$X_3 + X_4 = \frac{35\left(\phi_3 r^3 s^4 + \phi_4 r^4 s^3\right)}{\phi_0 s^7 + 7\phi_1 r^1 s^6 + 21\phi_2 r^2 s^5 + 35\phi_3 r^3 s^4 + 35\phi_4 r^4 s^3 + 21\phi_5 r^5 s^2 + 7\phi_6 r^6 s^1 + \phi_7 r^7}$$

The figure shows the results of a parametric non-linear least-squares fit of the heptamer model to the experimental data. The root mean square deviation between the heptamer model and data is 1.6%.

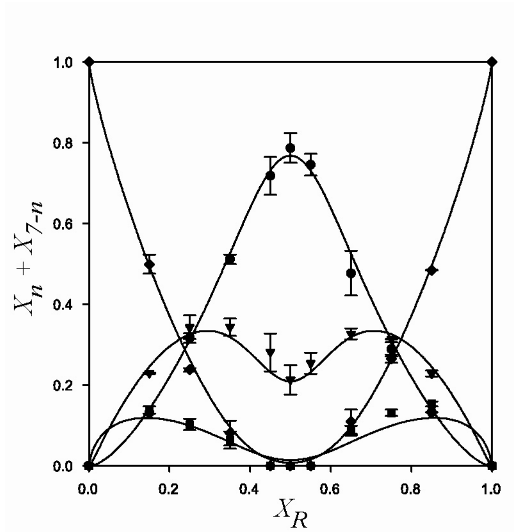

R_4S_3/R_3S_4 (●); R_2S_5/R_5S_2 (▾); R_1S_6/R_6S_1 (■); R_7/S_7 (◆).

Best fit values of φ

φ_0	φ_1	φ_2	φ_3	φ_4	φ_5	φ_6	φ_7
1.0	0.31	1.39	2.93	2.93	1.39	0.31	1.0

Percent Errors in φ_n

n	0	1	2	3
φ_n/φ_o	0	4.3	6.7	7.2
φ_n/φ_1	4.3	0	2.2	5.1
φ_n/φ_2	6.7	2.2	0	2.4
φ_n/φ_3	7.2	5.1	2.4	0

68. Generic tetramer Job plot. For the case where subunits A and B assemble into tetramers, the mole fraction of A, X_A, is related to the chemical potential using eqs 2-3.

$$X_A = \frac{\sum_{n=0}^{N} n\times M_n \times \phi_n \times a^n \times b^{N-n}}{\sum_{n=0}^{N} N\times M_n \times \phi_n \times a^n \times b^{N-n}} = \frac{\phi_1 a^1 b^3 + 3\phi_2 a^2 b^2 + 3\phi_3 a^3 b^1 + \phi_4 a^4}{\phi_0 b^4 + 4\phi_1 a^1 b^3 + 6\phi_2 a^2 b^2 + 4\phi_3 a^3 b^1 + \phi_4 a^4}$$

While the populations, X_n, are

$$X_0 = \frac{\phi_0 b^4}{\phi_0 b^4 + 4\phi_1 a^1 b^3 + 6\phi_2 a^2 b^2 + 4\phi_3 a^3 b^1 + \phi_4 a^4}$$

$$X_1 = \frac{4\phi_1 a^1 b^3}{\phi_0 b^4 + 4\phi_1 a^1 b^3 + 6\phi_2 a^2 b^2 + 4\phi_3 a^3 b^1 + \phi_4 a^4}$$

$$X_2 = \frac{6\phi_2 a^2 b^2}{\phi_0 b^4 + 4\phi_1 a^1 b^3 + 6\phi_2 a^2 b^2 + 4\phi_3 a^3 b^1 + \phi_4 a^4}$$

$$X_3 = \frac{4\phi_3 a^3 b^1}{\phi_0 b^4 + 4\phi_1 a^1 b^3 + 6\phi_2 a^2 b^2 + 4\phi_3 a^3 b^1 + \phi_4 a^4}$$

$$X_4 = \frac{\phi_4 a^4}{\phi_0 b^4 + 4\phi_1 a^1 b^3 + 6\phi_2 a^2 b^2 + 4\phi_3 a^3 b^1 + \phi_4 a^4}$$

The above formulae are used to plot all five populations as a function of X_A for a statistical distribution of species ($\varphi_0 = \varphi_1 = \ldots = \varphi_4$).

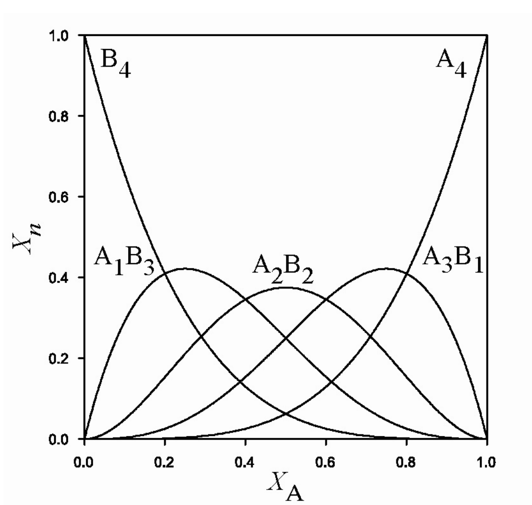

69. Dimer-tetramer Job plot. In this section we consider the case where two subunits, A and B, assemble to form species with different aggregation numbers (e.g., dimers and tetramers).

ϕ_{Nn} ($0 \le n \le N$) describes the mean free energy of N-mer aggregates with n subunits of A and N-n subunits of B.

$$[A_n B_{N-n}] = C \times M_n \times \phi_{Nn} \times a^n \times b^{N-n}$$

The concentration of [A] and [B] uniquely determine *a* and *b* by the implicit equations,

$$[A] = \sum_{N,n} n \times [A_n B_{N-n}] = \sum_{N,n} n \times C \times \frac{N!}{(N-n)! \times n!} \times \phi_{Nn} \times a^n \times b^{N-n}$$

$$[B] = \sum_{N,n} (N-n) \times [A_n B_{N-n}] = \sum_{N,n} (N-n) \times C \times \frac{N!}{(N-n)! \times n!} \times \phi_{Nn} \times a^n \times b^{N-n}$$

The mole fraction of $[A_nB_{N-n}]$, $X_{N,n}$, is given by

$$X_{Nn} = \frac{N \times [A_n B_{N-n}]}{[A]+[B]} = \frac{N \times \frac{N!}{(N-n)! \times n!} \times \phi_{Nn} \times a^n b^{N-n}}{\sum_{J,j} J \times \frac{J!}{(J-j)! \times j!} \times \phi_{Jj} \times a^j b^{J-j}}$$

For illustrative purposes, we consider the specific case of dimers and tetramers in equilibrium where species A forms dimers (A_2) and species B readily forms tetramers (B_4). Mixing A and B will give rise to a heterodimer (AB) and several heterotetramers (A_3B_1, A_2B_2, A_1B_3) in addition to the homodimer (A_2) and homotetramer (B_4).

The concentrations of [A] and [B] determine the values of *a* and *b* by the implicit equations,

$$[A] = C \times \left(2\phi_{21} a^1 b^1 + 2\phi_{22} a^2 + 4\phi_{41} a^1 b^3 + 12\phi_{42} a^2 b^2 + 12\phi_{43} a^3 b^1\right)$$

$$[B] = C \times \left(2\phi_{21} a^1 b^1 + 4\phi_{40} b^4 + 12\phi_{41} a^1 b^3 + 12\phi_{42} a^2 b^2 + 4\phi_{43} a^3 b^1\right)$$

The dimer mole fractions are given by,

$$X_{A_2} = \frac{2C\phi_{22}a^2}{[A]+[B]} \qquad X_{AB} = \frac{4C\phi_{21}a^1b^1}{[A]+[B]}$$

and the tetramer mole fractions are given by,

$$X_{A_3B_1} = \frac{16C\phi_{43}a^3b^1}{[A]+[B]} \qquad X_{A_2B_2} = \frac{24C\phi_{42}a^2b^2}{[A]+[B]}$$

$$X_{A_1B_3} = \frac{16C\phi_{41}a^1b^3}{[A]+[B]} \qquad X_{B_4} = \frac{4C\phi_{40}b^4}{[A]+[B]}$$

As one would anticipate, the relative aggregate populations depend on the mole fraction of A, X_A, and the total concentration of [A] and [B]. Qualitatively, increasing X_A will favor aggregates rich in A while increasing the overall concentration will favor the tetramers. Simultaneous fits of plots at several overall concentrations would provide more accurate free energies. For example, we have plotted representative plots for low (4), moderate (16) and high (100) total concentrations of [A] and [B] for a given set of ϕ_{Nn}.

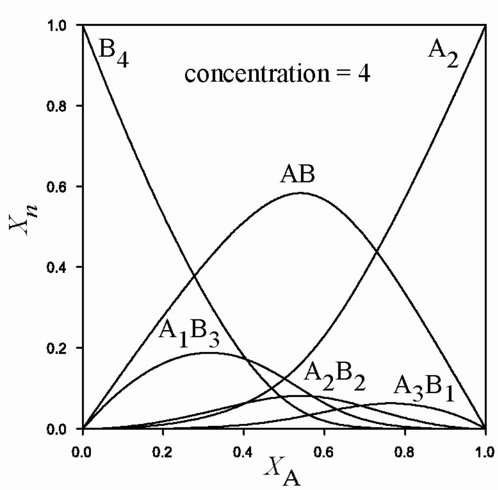

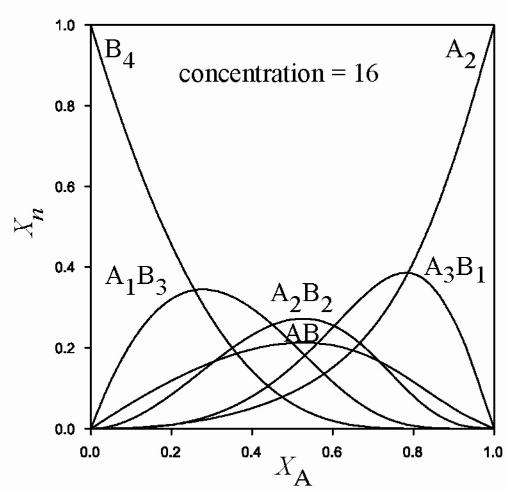

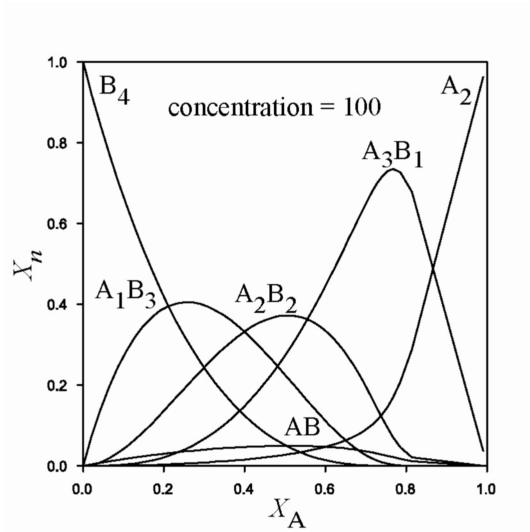

concentration = 100
B4
A2
A3B1
A1B3
A2B2
AB
Xn
XA
0.0
0.2
0.4
0.6
0.8
1.0